Ab initio many-body calculations of nucleon-nucleus scattering

Sofia Quaglioni and Petr Navrátil
Lawrence Livermore National Laboratory, P. O. Box 808, L-414, Livermore, California 94551, USA
(Received 7 January 2009; published 16 April 2009)

We develop a new *ab initio* many-body approach capable of describing simultaneously both bound and scattering states in light nuclei, by combining the resonating-group method with the use of realistic interactions, and a microscopic and consistent description of the nucleon clusters. This approach preserves translational symmetry and the Pauli principle. We outline technical details and present phase-shift results for neutron scattering on ^{3}H, ^{4}He, and ^{10}Be and proton scattering on ^{3,4}He, using realistic nucleon-nucleon (NN) potentials. Our $A = 4$ scattering results are compared to earlier *ab initio* calculations. We find that the CD-Bonn NN potential in particular provides an excellent description of nucleon-^{4}He S-wave phase shifts. In contrast, the experimental nucleon-^{4}He P-wave phase shifts are not well reproduced by any NN potential we use. We demonstrate that a proper treatment of the coupling to the n-^{10}Be continuum is successful in explaining the parity-inverted ground state in ^{11}Be.

DOI: 10.1103/PhysRevC.79.044606 PACS number(s): 21.60.De, 25.10.+s, 27.10.+h, 27.20.+n

I. INTRODUCTION

Nuclei are open quantum systems with bound states, unbound resonances, and scattering states. A realistic *ab initio* description of light nuclei with predictive power must have the capability to describe all these classes of states within a unified framework. Over the past decade, significant progress has been made in our understanding of the properties of the bound states of light nuclei starting from realistic nucleon-nucleon (NN) interactions (see, e.g., Ref. [1] and references therein) and more recently also from NN plus three-nucleon (NNN) interactions [2–4]. The solution of the nuclear many-body problem is even more complex when scattering or nuclear reactions are considered. For $A = 3$ and 4 nucleon systems, the Faddeev [5] and Faddeev-Yakubovsky [6] as well as the hyperspherical harmonics (HH) [7] or the Alt, Grassberger, and Sandhas (AGS) [8] methods are applicable and successful. However, *ab initio* calculations for scattering processes involving more than four nucleons overall are challenging and still a rare exception [9]. The development of an *ab initio* theory of low-energy nuclear reactions on light nuclei is key to further refining our understanding of the fundamental nuclear interactions among the constituent nucleons and providing, at the same time, accurate predictions of crucial reaction rates for nuclear astrophysics.

Recently, we combined the resonating-group method (RGM) [10–15] and the *ab initio* no-core shell model (NCSM) [16] into a new many-body approach [17] (*ab initio* NCSM/RGM) capable of treating bound and scattering states of light nuclei in a unified formalism, starting from the fundamental internucleon interactions. The RGM is a microscopic cluster technique based on the use of A-nucleon Hamiltonians, with fully antisymmetric many-body wave functions built by assuming that the nucleons are grouped into clusters. Although most of its applications are based on the use of binary-cluster wave functions, the RGM can be formulated for three (and, in principle, even more) clusters in relative motion [11]. The NCSM is an *ab initio* approach to the microscopic calculation of ground and low-lying excited states of light nuclei with realistic two- and, in general, three-nucleon forces. The use of the harmonic oscillator (HO) basis in the NCSM results in an incorrect description of the wave-function asymptotic and a lack of coupling to the continuum. The first applications of the NCSM to the calculation of nuclear reactions required a phenomenological correction of the asymptotic behavior of the overlap functions [18]. In contrast, the present approach is fully *ab initio*. We complement the ability of the RGM to deal with scattering and reactions with the use of realistic interactions and a consistent *ab initio* description of the nucleon clusters, achieved via the NCSM. Presently, the NCSM/RGM approach has been formulated for processes involving binary-cluster systems only, and thus it is appropriate for the description of low-energy reactions below three-body breakup threshold. However, extensions of the approach to include three-body cluster channels are feasible, also in view of recent developments on the treatment of both three-body bound and continuum states (see, e.g., Refs. [19–23]). Within the *ab initio* NCSM/RGM approach we studied the n-^{3}H, n-^{4}He, n-^{10}Be, and p-^{3,4}He scattering processes and addressed the parity inversion of the ^{11}Be ground state (g.s.), using realistic NN potentials [17]. In this paper, we give the technical details of these calculations, discuss results published in Ref. [17] more extensively, and present additional results.

In Sec. II, we present technical details of our approach. We give two independent derivations of the NCSM/RGM kernels, discuss orthogonalization of the RGM equations, and give illustrative examples of the kernels. Results of *ab initio* NCSM/RGM applications to $A = 4$, $A = 5$, and $A = 11$ systems are given in Sec. III. Conclusions are drawn in Sec. IV and some of the most complex derivations are summarized in Appendix A.

II. FORMALISM

The wave function for a scattering process involving pairs of nuclei can be cast in the form

$$|\Psi^{J^\pi T}\rangle = \sum_\nu \int dr\, r^2 \frac{g_\nu^{J^\pi T}(r)}{r} \hat{\mathcal{A}}_\nu \left|\Phi_{\nu r}^{J^\pi T}\right\rangle, \qquad (1)$$

through an expansion over binary-cluster channel states of total angular momentum J, parity π, and isospin T,

$$\left|\Phi^{J^\pi T}_{\nu r}\right\rangle = \left[\left(\left|A{-}a\ \alpha_1 I_1^{\pi_1} T_1\right\rangle \left|a\ \alpha_2 I_2^{\pi_2} T_2\right\rangle\right)^{(sT)} Y_\ell(\hat{r}_{A-a,a})\right]^{(J^\pi T)} \times \frac{\delta(r - r_{A-a,a})}{r r_{A-a,a}}. \quad (2)$$

The internal wave functions of the colliding nuclei (which we will often refer to as clusters), contain $A-a$ and a nucleons ($a < A$), respectively, are antisymmetric under exchange of internal nucleons, and depend on translationally invariant internal coordinates. They are eigenstates of $H_{(A-a)}$ and $H_{(a)}$, the $(A-a)$- and a-nucleon intrinsic Hamiltonians, respectively, with angular momentum quantum numbers I_1 and I_2 coupled together to form channel spin s. For their parity, isospin, and additional quantum numbers we use, respectively, the notations π_i, T_i, and α_i, with $i = 1, 2$. The channel states [Eq. (2)] have relative angular momentum ℓ. If we denote the A single-particle coordinates with $\{\vec{r}_i, i = 1, 2, \ldots, A\}$, the clusters' centers of mass are separated by the relative vector

$$\vec{r}_{A-a,a} = r_{A-a,a}\hat{r}_{A-a,a} = \frac{1}{A-a}\sum_{i=1}^{A-a}\vec{r}_i - \frac{1}{a}\sum_{j=A-a+1}^{A}\vec{r}_j. \quad (3)$$

The symbols Y_ℓ and δ denote a spherical harmonic and a Dirac delta, respectively. The intercluster antisymmetrizer for the $(A-a, a)$ partition in Eq. (1) can be schematically written as $\hat{\mathcal{A}}_\nu = [(A-a)!a!/A!]^{1/2}\sum_P(-)^p P$, where P are permutations among nucleons pertaining to different clusters, and p is the number of interchanges characterizing them. The coefficients of the expansion with respect to the channel index $\nu = \{A{-}a\ \alpha_1 I_1^{\pi_1} T_1; a\ \alpha_2 I_2^{\pi_2} T_2; s\ell\}$ are the relative-motion wave functions $g_\nu^{J^\pi T}(r)$, which represent the unknowns of the problem. They can be determined by solving the many-body Schrödinger equation in the Hilbert space spanned by the basis states $\hat{\mathcal{A}}_\nu \left|\Phi^{J^\pi T}_{\nu r}\right\rangle$:

$$\sum_\nu \int dr\, r^2 \left[\mathcal{H}^{J^\pi T}_{\nu'\nu}(r', r) - E\,\mathcal{N}^{J^\pi T}_{\nu'\nu}(r', r)\right]\frac{g_\nu^{J^\pi T}(r)}{r} = 0, \quad (4)$$

where

$$\mathcal{H}^{J^\pi T}_{\nu'\nu}(r', r) = \left\langle \Phi^{J^\pi T}_{\nu' r'} \middle| \hat{\mathcal{A}}_{\nu'} H \hat{\mathcal{A}}_\nu \middle| \Phi^{J^\pi T}_{\nu r} \right\rangle, \quad (5)$$

$$\mathcal{N}^{J^\pi T}_{\nu'\nu}(r', r) = \left\langle \Phi^{J^\pi T}_{\nu' r'} \middle| \hat{\mathcal{A}}_{\nu'} \hat{\mathcal{A}}_\nu \middle| \Phi^{J^\pi T}_{\nu r} \right\rangle \quad (6)$$

are called the Hamiltonian and norm kernels, respectively. Here E is the total energy in the center-of-mass (c.m.) frame, and H is the intrinsic A-nucleon microscopic Hamiltonian, for which it is useful to use the decomposition

$$H = T_{\rm rel}(r) + \mathcal{V}_{\rm rel} + \bar{V}_C(r) + H_{(A-a)} + H_{(a)}. \quad (7)$$

Further, $T_{\rm rel}(r)$ is the relative kinetic energy and $\mathcal{V}_{\rm rel}$ is the sum of all interactions between nucleons belonging to different clusters after subtraction of the average Coulomb interaction between them, explicitly singled out in the term $\bar{V}_C(r) = Z_{1\nu}Z_{2\nu}e^2/r$, where $Z_{1\nu}$ and $Z_{2\nu}$ are the charge numbers of the clusters in channel ν:

$$\begin{aligned}\mathcal{V}_{\rm rel} &= \sum_{i=1}^{A-a}\sum_{j=A-a+1}^{A} V_{ij} + \mathcal{V}^{3N}_{(A-a,a)} - \bar{V}_C(r) \\ &= \sum_{i=1}^{A-a}\sum_{j=A-a+1}^{A}\left[V_N(\vec{r}_i - \vec{r}_j, \sigma_i, \sigma_j, \tau_i, \tau_j)\right. \\ &\quad \left. + \frac{e^2\left(1+\tau_i^z\right)\left(1+\tau_j^z\right)}{4|\vec{r}_i - \vec{r}_j|} - \frac{1}{(A-a)a}\bar{V}_C(r)\right] \\ &\quad + \mathcal{V}^{3N}_{(A-a,a)}. \end{aligned} \quad (8)$$

In this expression we explicitly distinguished among nucleon-nucleon, nuclear (V_N) plus Coulomb (point and average), and three-nucleon ($\mathcal{V}^{3N}_{(A-a,a)}$) components of the intercluster interaction. The contribution from the nuclear interaction vanishes exponentially for increasing distances between particles. Because of the subtraction of $V_C(r)$, the overall Coulomb contribution presents a r^{-2} behavior, as the distance r between the two clusters increases. Therefore, $\mathcal{V}_{\rm rel}$ is localized also in the presence of the Coulomb force. In the present paper we will consider only the NN part of the intercluster interaction and disregard, for the time being, the term $\mathcal{V}^{3N}_{(A-a,a)}$. The inclusion of the three-nucleon force into the formalism, although more involved, is straightforward and will be the matter of future investigations. Finally, although in Eq. (8) the strong part of the NN force (V_N) is represented as a local potential, this separation of the Hamiltonian as well as the rest of the formalism presented throughout this paper is valid also in the presence of a nonlocal potential.

A. Cluster eigenstate calculation

We obtain the cluster eigenstates entering Eq. (2) by diagonalizing $H_{(A-a)}$ and $H_{(a)}$ in the model space spanned by the NCSM basis. This is a complete HO basis, the size of which is defined by the maximum number, $N_{\rm max}$, of HO quanta above the lowest configuration shared by the nucleons. (The definition of the model-space size coincides for eigenstates of the same parity but differs by one unit for eigenstates of opposite parity; the same HO frequency Ω is used for both clusters.) If the NN (or NNN) potential used in the calculation generates strong short-range correlations, which is typical for standard accurate NN potentials, the $H_{(A-a)}$ and $H_{(a)}$ Hamiltonians are treated as NCSM effective Hamiltonians, tailored to the $N_{\rm max}$ truncation, obtained by employing the usual NCSM effective interaction techniques [4,16]. The effective interactions are derived from the underlying NN and, in general, three-nucleon potential models (not included in the present investigations) through a unitary transformation in a way that guarantees convergence to the exact solution as the model-space size increases. However, if low-momentum NN potentials, which have high-momentum components already transformed away by unitary transformations, are employed in the calculations, the $H_{(A-a)}$ and $H_{(a)}$ Hamiltonians are taken un-renormalized or "bare."

The unique properties of the HO basis allow us to make use of Jacobi-coordinate wave functions [24,25] for both nuclei, or only for the lightest of the pair (typically $a \leqslant 4$) referenced further on as projectile, and still preserve the translational invariance of the problem. In the second case we expand the eigenstates of the heavier cluster (target) on a Slater-determinant (SD) basis and remove completely the spurious c.m. components in a similar fashion as in Refs. [18,26,27]. We exploited this dual approach to verify our results. The use of the SD basis is computationally advantageous and allows us to explore reactions involving p-shell nuclei.

B. Interaction between nucleons belonging to different clusters

In calculating Eqs. (5) and (6), all "direct" terms arising from the identical permutations in both $\hat{\mathcal{A}}_\nu$ and $\hat{\mathcal{A}}_{\nu'}$ are treated exactly (with respect to the separation r) with the exception of $\langle \Phi^{J^\pi T}_{\nu' r'} | \mathcal{V}_{\rm rel} | \Phi^{J^\pi T}_{\nu r} \rangle$. The latter and all remaining terms are localized and can be obtained by expanding the Dirac δ of Eq. (2) on a set of HO radial wave functions with identical frequency Ω, and model-space size $N_{\rm max}$ consistent with those used for the two clusters. The rate of convergence of these terms is closely related to the nuclear force model adopted in the Hamiltonian [Eq. (7)]. For most nuclear interaction models that generate strong short-range nucleon-nucleon correlations the large but finite model spaces computationally achievable are insufficient to reach the full convergence through a "bare" calculation. In these cases it is crucial to utilize effective interactions tailored to the truncated model spaces. In our approach the effective interactions are derived from the underlying NN potential through a unitary transformation, as already pointed out in the previous section. The cluster eigenstates are obtained by employing the usual NCSM effective interaction [16], whereas in place of the bare NN nuclear potential V_N entering $\mathcal{V}_{\rm rel}$ [Eq. (8)] we adopt a modified two-body effective interaction, $V'_{2\rm eff}$, that avoids renormalizations related to the kinetic energy. The kinetic-energy renormalizations are appropriate within the standard NCSM, but they would compromise scattering results obtained within the NCSM/RGM approach, in which the relative kinetic energy and the average Coulomb interaction between the clusters are treated exactly. More specifically, in addition to the relevant two-nucleon Hamiltonian (see also Refs. [16,25])

$$H_2^\Omega = H_{02} + V_{12} = \frac{\vec{p}^{\,2}}{2m} + \frac{1}{2} m\Omega^2 \vec{x}^{\,2} + V_N(\sqrt{2}\vec{x}) - \frac{m\Omega^2}{A}\vec{x}^{\,2}, \tag{9}$$

where $\vec{x} = \sqrt{\frac{1}{2}}(\vec{r}_1 - \vec{r}_2)$ and $\vec{p} = \sqrt{\frac{1}{2}}(\vec{p}_1 - \vec{p}_2)$, we introduce here a second, modified two-nucleon Hamiltonian, deprived of the nuclear interaction:

$$H_2'^{\Omega} = H_{02} + V'_{12} = \frac{\vec{p}^{\,2}}{2m} + \frac{1}{2} m\Omega^2 \vec{x}^{\,2} - \frac{m\Omega^2}{A}\vec{x}^{\,2}. \tag{10}$$

The modified two-body effective interaction is then determined from the two-nucleon Hermitian effective Hamiltonians $\bar{H}_{2\rm eff}$ and $\bar{H}'_{2\rm eff}$, obtained via the Lee-Suzuki similarity transformation method [28] starting from Eqs. (9) and (10), respectively:

$$V'_{2\rm eff} = \bar{H}_{2\rm eff} - \bar{H}'_{2\rm eff}. \tag{11}$$

We note that (i) $V'_{2\rm eff} \to V_N$ in the limit $N_{\rm max} \to \infty$ and (ii) for each model space, the renormalizations related to the kinetic energy and the HO potential introduced in $\bar{H}_{2\rm eff}$ are compensated by the subtraction of $\bar{H}'_{2\rm eff}$.

C. Coordinates and basis states

We neglect the difference between proton and neutron masses and denote the average nucleon mass with m. The formalism presented in this paper is based both on the single-particle Cartesian coordinates, $\{\vec{r}_i, i = 1, 2, \ldots, A\}$, and on the following set of Jacobi coordinates:

$$\vec{\xi}_0 = \sqrt{\frac{1}{A}} \sum_{i=1}^{A} \vec{r}_i, \tag{12}$$

the vector proportional to the center of mass (c.m.) coordinate of the A-nucleon system ($R_{\rm c.m.} = \frac{1}{\sqrt{A}}\vec{\xi}_0$);

$$\begin{aligned} \vec{\xi}_1 &= \sqrt{\frac{1}{2}}(\vec{r}_1 - \vec{r}_2), \\ \vec{\xi}_k &= \sqrt{\frac{k}{k+1}} \left[\frac{1}{k} \sum_{i=1}^{k} \vec{r}_i - \vec{r}_{k+1} \right], \quad 2 \leqslant k \leqslant A - a - 1\,; \end{aligned} \tag{13}$$

the translationally invariant internal coordinates for the first $A - a$ nucleons;

$$\vec{\eta}_{A-a} = \sqrt{\frac{(A-a)a}{A}} \left[\frac{1}{A-a} \sum_{i=1}^{A-a} \vec{r}_i - \frac{1}{a} \sum_{j=A-a+1}^{A} \vec{r}_j \right], \tag{14}$$

the vector proportional to the relative position between the c.m. of the two clusters ($\vec{r}_{A-a,a} = \sqrt{\frac{A}{(A-a)a}}\vec{\eta}_{A-a}$); and, finally,

$$\begin{aligned} \vec{\vartheta}_{A-k} &= \sqrt{\frac{k}{k+1}} \left[\frac{1}{k} \sum_{i=1}^{k} \vec{r}_{A-i+1} - \vec{r}_{A-k} \right], \quad a - 1 \geqslant k \geqslant 2, \\ \vec{\vartheta}_{A-1} &= \sqrt{\frac{1}{2}}(\vec{r}_{A-1} - \vec{r}_A), \end{aligned} \tag{15}$$

the translationally invariant internal coordinates for the last a nucleons.

1. *Jacobi basis*

Nuclei are translationally invariant systems. Therefore, the use of Jacobi coordinates and translationally invariant basis states represents a "natural" choice for the solution of the many-nucleon problem.

In working with the Jacobi relative coordinates of Eqs. (13), (14), and (16), it is convenient to introduce the (translationally invariant) Jacobi channel states

$$\begin{aligned} \left| \Phi^{J^\pi T}_{\nu\eta} \right\rangle = \left[\left(\left| A{-}a\ \alpha_1 I_1^{\pi_1} T_1 \right\rangle \left| a\ \alpha_2 I_2^{\pi_2} T_2 \right\rangle \right)^{(sT)} Y_\ell(\hat{\eta}_{A-a}) \right]^{(J^\pi T)} \\ \times \frac{\delta(\eta - \eta_{A-a})}{\eta \eta_{A-a}}, \end{aligned} \tag{16}$$

which are clearly proportional to the binary-cluster basis presented in Eq. (2):

$$\left|\Phi^{J^\pi T}_{\nu r}\right\rangle = \left[\frac{(A-a)a}{A}\right]^{3/2} \left|\Phi^{J^\pi T}_{\nu\eta}\right\rangle. \tag{17}$$

The clusters' intrinsic wave functions depend on their respective set of Jacobi, spin (σ), and isospin (τ) coordinates,

$$\left\langle \vec{\xi}_1 \cdots \vec{\xi}_{A-a-1}\sigma_1 \cdots \sigma_{A-a}\tau_1 \cdots \tau_{A-a}\middle| A{-}a\ \alpha_1 I_1^{\pi_1} T_1\right\rangle, \tag{18}$$

$$\left\langle \vec{\vartheta}_{A-a+1} \cdots \vec{\vartheta}_{A-1}\sigma_{A-a+1} \cdots \sigma_A\tau_{A-a+1} \cdots \tau_A\middle| a\ \alpha_2 I_2^{\pi_2} T_2\right\rangle, \tag{19}$$

and are obtained by diagonalizing the $H_{(A-a)}$ and $H_{(a)}$ intrinsic Hamiltonians in the model spaces spanned by the NCSM Jacobi-coordinate basis [25]. The same HO frequency Ω is used for both clusters. The model-space size coincides for eigenstates of the same parity and differs by one unit for eigenstates of opposite parity.

In calculating the integral kernels of Eqs. (5) and (6), $\langle\Phi^{J^\pi T}_{\nu' r'}|\mathcal{V}_{\rm rel}|\Phi^{J^\pi T}_{\nu r}\rangle$ and all "exchange" terms, arising from the permutations in $\mathcal{A}_\nu$ or $\mathcal{A}_{\nu'}$ different from the identity, are obtained by expanding the Dirac δ of Eq. (2) on a set of HO radial wave functions with identical frequency Ω and model-space size $N_{\rm max}$ consistent with those used for the two clusters:

$$\left|\Phi^{J^\pi T}_{\nu r}\right\rangle = \left[\frac{(A-a)a}{A}\right]^{3/2} \sum_n R_{n\ell}(\eta, b_0)\left|\Phi^{J^\pi T}_{\nu n, b_0}\right\rangle \tag{20}$$

$$= \sum_n R_{n\ell}(r, b)\left|\Phi^{J^\pi T}_{\nu n, b}\right\rangle, \tag{21}$$

where the HO Jacobi channel states are given by

$$\left|\Phi^{J^\pi T}_{\nu n, b}\right\rangle = \left[\left(\left|A{-}a\ \alpha_1 I_1^{\pi_1} T_1\right\rangle \left|a\ \alpha_2 I_2^{\pi_2} T_2\right\rangle\right)^{(sT)} Y_\ell(\hat{\eta}_{A-a})\right]^{(J^\pi T)} \times R_{n\ell}(r_{A-a,a}, b) \tag{22}$$

$$= \left[\sqrt{\frac{(A-a)a}{A}}\right]^{3/2} \left|\Phi^{J^\pi T}_{\nu n, b_0}\right\rangle. \tag{23}$$

Note that the HO basis states depending on the Jacobi coordinates introduced in Sec. II C are all characterized by the same oscillator-length parameter $b_0 = \sqrt{\hbar/m\Omega}$. However, the oscillator-length parameter associated with the separation r between the centers of mass of target and projectile is defined in terms of the reduced mass $\mu = [(A-a)a\,m]/A$ of the channel under consideration: $b = \sqrt{\hbar/\mu\Omega} = \sqrt{A/[(A-a)a]}\,b_0$. In the following we will drop the explicit reference to the HO length parameter in the arguments of the HO radial wave functions and in the HO Jacobi channel states $|\Phi^{J^\pi T}_{\nu n}\rangle$.

2. Single-particle Slater-determinant basis

The unique properties of the HO basis allow us to make use of Jacobi-coordinate wave functions [24,25] for both nuclei or only for the lighter of the pair (typically $a \leqslant 4$) and still preserve the translational invariance of the problem (see also the discussions in Refs. [26,27]). In the second case we introduce the SD channel states

$$\left|\Phi^{J^\pi T}_{\nu n}\right\rangle_{\rm SD} = \left[\left(\left|A{-}a\ \alpha_1 I_1 T_1\right\rangle_{\rm SD}\left|a\ \alpha_2 I_2 T_2\right\rangle\right)^{(sT)} Y_\ell\left(\hat{R}^{(a)}_{\rm c.m.}\right)\right]^{(J^\pi T)} \times R_{n\ell}\left(R^{(a)}_{\rm c.m.}\right), \tag{24}$$

in which the eigenstates of the $(A-a)$-nucleon fragment are obtained in the SD basis,

$$\left\langle \vec{r}_1 \cdots \vec{r}_{A-a}\sigma_1 \cdots \sigma_{A-a}\tau_1 \cdots \tau_{A-a}\middle| A{-}a\ \alpha_1 I_1^{\pi_1} T_1\right\rangle_{\rm SD}, \tag{25}$$

that is, by using a shell-model code (such as, e.g., ANTOINE [29] or MFD [30]), and contain therefore the spurious motion of the $(A-a)$-nucleon cluster c.m. The SD and Jacobi-coordinate eigenstates are related by the expression

$$|A{-}a\ \alpha_1 I_1 T_1\rangle_{\rm SD} = |A{-}a\ \alpha_1 I_1 T_1\rangle\ \varphi_{00}\left(\vec{R}^{(A-a)}_{\rm c.m.}\right). \tag{26}$$

The c.m. coordinates introduced in Eqs. (24) and (26),

$$\vec{R}^{(A-a)}_{\rm c.m.} = \sqrt{\frac{1}{A-a}}\sum_{i=1}^{A-a}\vec{r}_i; \quad \vec{R}^{(a)}_{\rm c.m.} = \sqrt{\frac{1}{a}}\sum_{i=A-a+1}^{A}\vec{r}_i, \tag{27}$$

are an orthogonal transformation of the c.m. and relative coordinates of the A-nucleon system, $\vec{\xi}_0$ (12) and $\vec{\eta}_{A-a}$ (14), respectively:

$$\vec{\eta}_{A-a} = \sqrt{\frac{a}{A}}\vec{R}^{(A-a)}_{\rm c.m.} - \sqrt{\frac{A-a}{A}}\vec{R}^{(a)}_{\rm c.m.}, \tag{28}$$

$$\vec{\xi}_0 = \sqrt{\frac{A-a}{A}}\vec{R}^{(A-a)}_{\rm c.m.} + \sqrt{\frac{a}{A}}\vec{R}^{(a)}_{\rm c.m.}. \tag{29}$$

Therefore, in the SD basis of Eq. (24), the HO wave functions depending on these coordinates transform according to

$$\left(\varphi_{00}\left(\vec{R}^{(A-a)}_{\rm c.m.}\right)\varphi_{n\ell}\left(\vec{R}^{(a)}_{\rm c.m.}\right)\right)^{(\ell)} = \sum_{n_r\ell_r,NL}\langle 00n\ell\ell|n_r\ell_r NL\ell\rangle_{\frac{a}{A-a}}\left(\varphi_{n_r\ell_r}(\vec{\eta}_{A-a})\,\varphi_{NL}(\vec{\xi}_0)\right)^{(\ell)}, \tag{30}$$

where the coefficients of the expansion are generalized HO brackets for two particles with mass ratio $d = \frac{a}{A-a}$ that can be calculated as described, for example, in Ref. [31]. As a result the SD and Jacobi channel states are related by

$$\left|\Phi^{J^\pi T}_{\nu n}\right\rangle_{\rm SD} = \sum_{n_r\ell_r,NL,J_r}\hat{\ell}\hat{J}_r\,(-1)^{(s+\ell_r+L+J)} \times \begin{Bmatrix} s & \ell_r & J_r \\ L & J & \ell \end{Bmatrix}\langle n_r\ell_r NL\ell|00n\ell\ell\rangle_{\frac{a}{A-a}} \times \left[\left|\Phi^{J^{\pi_r}_r T}_{\nu_r n_r}\right\rangle\varphi_{NL}(\vec{\xi}_0)\right]^{(J^\pi T)}, \tag{31}$$

where $\nu_r = \{A{-}a\ \alpha_1 I_1 T_1; a\ \alpha_2 I_2 T_2; s\ell_r\}$. It is therefore possible to extract the translationally invariant matrix elements from those calculated in the SD basis, which contain the spurious c.m. motion, by inverting the following expression:

$${}_{\rm SD}\left\langle\Phi^{J^\pi T}_{\nu' n'}\middle|\hat{\mathcal{O}}_{\rm t.i.}\middle|\Phi^{J^\pi T}_{\nu n}\right\rangle_{\rm SD} = \sum_{n'_r\ell'_r,n_r\ell_r,J_r}\left\langle\Phi^{J^{\pi_r}_r T}_{\nu'_r n'_r}\middle|\hat{\mathcal{O}}_{\rm t.i.}\middle|\Phi^{J^{\pi_r}_r T}_{\nu_r n_r}\right\rangle$$

$$\times \sum_{NL} \hat{\ell}\hat{\ell}'\hat{J}_r^2(-1)^{(s+\ell-s'-\ell')} \begin{Bmatrix} s & \ell_r & J_r \\ L & J & \ell \end{Bmatrix} \begin{Bmatrix} s' & \ell'_r & J_r \\ L & J & \ell' \end{Bmatrix}$$
$$\times \langle n_r \ell_r N L \ell | 00 n \ell \ell \rangle_{\frac{a}{A-a}} \langle n'_r \ell'_r N L \ell | 00 n' \ell' \ell' \rangle_{\frac{a}{A-a}}, \quad (32)$$

where $\hat{\mathcal{O}}_{\text{t.i.}}$ is any scalar and parity-conserving translational-invariant operator ($\hat{\mathcal{O}}_{\text{t.i.}} = \hat{\mathcal{A}}$, $\hat{\mathcal{A}}H\hat{\mathcal{A}}$, etc.).

We exploited this dual approach to verify our results. The use of the SD basis is computationally advantageous and allows us to explore reactions involving p-shell nuclei.

D. Translational invariant kernels in the single-nucleon-projectile basis

All calculations in the present paper were carried out in the single-nucleon projectile (SNP) basis, that is, using binary-cluster channels [Eq. (2)] with $a = 1$. In this case, the ϑ coordinates are not defined, the channel index reduces to $\nu = \{A{-}1\ \alpha_1 I_1^{\pi_1} T_1; 1\frac{1}{2}\frac{1}{2}; s\ell\}$, and the intercluster antisymmetrizer is simply given by

$$\hat{\mathcal{A}}_\nu \equiv \hat{\mathcal{A}} = \frac{1}{\sqrt{A}} \left[1 - \sum_{i=1}^{A-1} \hat{P}_{iA} \right]. \quad (33)$$

In calculating Eqs. (5) and (6), it is convenient to isolate the "direct" terms arising from the identical permutation in $\hat{\mathcal{A}}$. Considering that the full A-nucleon Hamiltonian commutes with the intercluster antisymmetrizer ($[\hat{\mathcal{A}}, H] = 0$), and that

$$\hat{\mathcal{A}}^2 \left| \Phi_{\nu r}^{J^\pi T} \right\rangle = \left[1 - \sum_{i=1}^{A-1} \hat{P}_{iA} \right] \left| \Phi_{\nu r}^{J^\pi T} \right\rangle, \quad (34)$$

we can write the following expression for the norm kernel in the SNP basis:

$$\mathcal{N}_{\nu'\nu}^{J^\pi T}(r', r) = \delta_{\nu'\nu} \frac{\delta(r'-r)}{r'r} + \mathcal{N}_{\nu'\nu}^{\text{ex}}(r', r). \quad (35)$$

Here, we have singled out the nonlocal exchange part of the matrix elements in the term

$$\mathcal{N}_{\nu'\nu}^{\text{ex}}(r', r) = -\left\langle \Phi_{\nu' r'}^{J^\pi T} \right| \sum_{i=1}^{A-1} \hat{P}_{iA} \left| \Phi_{\nu r}^{J^\pi T} \right\rangle \quad (36)$$
$$= -(A-1) \sum_{n'n} R_{n'\ell'}(r') R_{n\ell}(r)$$
$$\times \left\langle \Phi_{\nu' n'}^{J^\pi T} \right| \hat{P}_{A-1,A} \left| \Phi_{\nu n}^{J^\pi T} \right\rangle \quad (37)$$

(and have dropped for simplicity the $J^\pi T$ superscript). In the schematic representation of the norm kernel of Fig. 1, diagram (a) and (b) correspond to the first and second terms, respectively, of the right hand side of Eq. (35).

In deriving Eq. (37) we used the expansion given by Eq. (21) and took advantage of the internal symmetry properties of the $(A-1)$-cluster wave function. A similar decomposition can be performed also for the Hamiltonian kernel,

$$\mathcal{H}_{\nu'\nu}^{J^\pi T}(r', r) = \left\langle \Phi_{\nu' r'}^{J^\pi T} \right| H \left[1 - \sum_{i=1}^{A-1} \hat{P}_{iA} \right] \left| \Phi_{\nu r}^{J^\pi T} \right\rangle \quad (38)$$

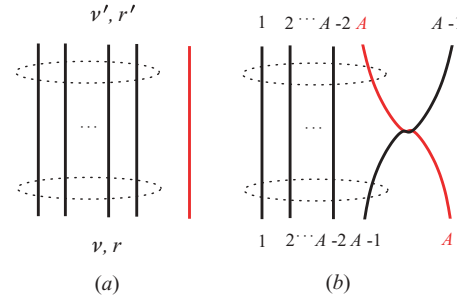

FIG. 1. (Color online) Diagrammatic representation of the "direct" (a) and "exchange" (b) components of the norm kernel. The first group of circled black lines represents the first cluster, the bound state of $A-1$ nucleons. The separate red line represents the second cluster, in the specific case of a single nucleon. The lower and upper parts of the diagram represent initial and final states, respectively.

$$= \left[\hat{T}_{\text{rel}}(r') + \bar{V}_C(r') + E_{\alpha'_1}^{I_1^{\pi_1'} T_1'} \right] \mathcal{N}_{\nu'\nu}^{J^\pi T}(r', r)$$
$$+ \mathcal{V}_{\nu'\nu}^{\text{D}}(r', r) + \mathcal{V}_{\nu'\nu}^{\text{ex}}(r', r), \quad (39)$$

where we divided $\langle \Phi_{\nu' r'}^{J^\pi T} | \mathcal{V}_{\text{rel}} \hat{\mathcal{A}}^2 | \Phi_{\nu r}^{J^\pi T} \rangle$ into "direct" and "exchange" potential kernels according to

$$\mathcal{V}_{\nu'\nu}^{\text{D}}(r', r) = (A-1) \sum_{n'n} R_{n'\ell'}(r') R_{n\ell}(r)$$
$$\times \left\langle \Phi_{\nu' n'}^{J^\pi T} \right| V_{A-1,A}(1 - \hat{P}_{A-1,A}) \left| \Phi_{\nu n}^{J^\pi T} \right\rangle, \quad (40)$$

$$\mathcal{V}_{\nu'\nu}^{\text{ex}}(r', r) = -(A-1)(A-2) \sum_{n'n} R_{n'\ell'}(r') R_{n\ell}(r)$$
$$\times \left\langle \Phi_{\nu' n'}^{J^\pi T} \right| \hat{P}_{A-1,A} V_{A-2,A-1} \left| \Phi_{\nu n}^{J^\pi T} \right\rangle. \quad (41)$$

Diagrams (c) and (d) of Fig. 2 give a schematic view of Eq. (40), whereas Eq. (41) corresponds to diagram (e). As pointed out in Sec. II, the channel states [Eq. (2)] are not antisymmetric with respect to the exchange of nucleons pertaining to different clusters (fully antisymmetric states are recovered through the action of the operator $\hat{\mathcal{A}}_\nu$). As a consequence, the Hamiltonian kernel as defined in Eq. (38) is explicitly non-Hermitian. Using $\hat{\mathcal{A}}H\hat{\mathcal{A}} = \frac{1}{2}(\hat{\mathcal{A}}^2 H + H\hat{\mathcal{A}}^2)$, we introduce the Hermitized Hamiltonian kernel $\bar{\mathcal{H}}_{\nu'\nu}^{J^\pi T}$ in the form

$$\bar{\mathcal{H}}_{\nu'\nu}^{J^\pi T}(r', r) = \left\langle \Phi_{\nu' r'}^{J^\pi T} \right| H - \frac{1}{2} \sum_{i=1}^{A-1} (H \hat{P}_{iA} + \hat{P}_{iA} H) \left| \Phi_{\nu r}^{J^\pi T} \right\rangle. \quad (42)$$

Finally, we note that, according to Eqs. (7) and (8) and Eqs. (35) and (37), the contribution of the average Coulomb potential to the Hermitian Hamiltonian kernel [Eq. (42)] amounts overall to

$$\frac{1}{2} \delta_{\nu'\nu} [\bar{V}_C(r') + \bar{V}_C(r)] \left[\frac{\delta(r'-r)}{r'r} - \sum_n R_{n\ell}(r') R_{n\ell}(r) \right]. \quad (43)$$

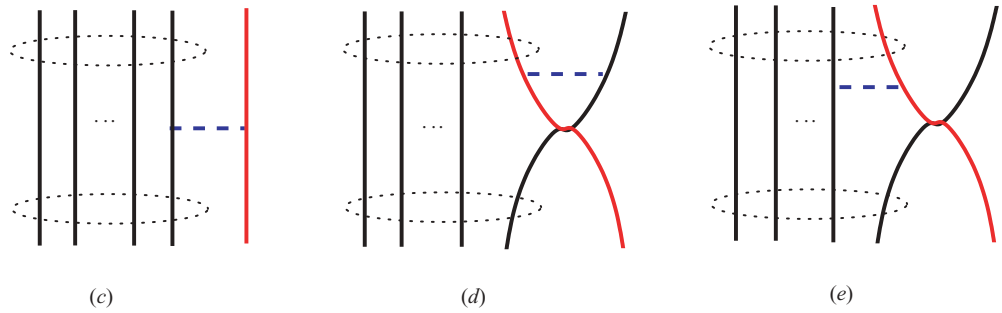

FIG. 2. (Color online) Diagrammatic representation of "direct" (c and d) and "exchange" (e) components of the potential kernel (see also the caption of Fig. 1).

1. Jacobi-coordinate derivation

The main technical as well as computational challenge of the NCSM/RGM approach lies in the evaluation of norm and Hamiltonian kernels. The analytical expressions for the integral kernels of Eqs. (37), (40), and (41) assume a particularly involved aspect in the model space spanned by the HO Jacobi channel states of Eq. (22). Here we discuss the exchange part of the norm kernel for the $A = 3$ system ($a = 1$), which is representative of the Jacobi-coordinate formalism without requiring overly tedious manipulations. Interested readers can find a compilation of all Jacobi-coordinate formulas, along with an outline of their derivation, in Appendix A.

The HO Jacobi channel state of Eq. (22) for the (2, 1) partition can be written as

$$\left|\Phi^{J^\pi T}_{\nu,n}\right\rangle = \sum_{n_1\ell_1 s_1} \left\langle n_1\ell_1 s_1 I_1 T_1 \middle| 2\,\alpha_1 I_1^{\pi_1} T_1\right\rangle \times \left|\left[\left(n_1\ell_1 s_1 I_1 T_1; \frac{1}{2}\frac{1}{2}\right) sT; n\ell\right] J^\pi T\right\rangle, \quad (44)$$

where we have expanded the two-nucleon target wave function onto HO basis states depending on the Jacobi coordinate $\vec{\xi}_1$ defined in Eq. (13),

$$\langle \vec{\xi}_1 \sigma_1\sigma_2\tau_1\tau_2 | n_1\ell_1 s_1 I_1 T_1\rangle, \quad (45)$$

and $\langle n_1\ell_1 s_1 I_1 T_1 | 2\,\alpha_1 I_1^{\pi_1} T_1\rangle$ are the coefficients of the expansion. Here n_1 and ℓ_1 are the HO quantum numbers corresponding to the harmonic oscillator associated with $\vec{\xi}_1$, and s_1, I_1, and T_1 are the spin, total angular momentum, and isospin of the two-nucleon channel formed by nucleons 1 and 2, respectively. Note that the basis [Eq. (45)] is antisymmetric with respect to the exchange of the two nucleons: $(-)^{\ell_1+s_1+T_1} = -1$.

According to Eq. (37), to obtain the exchange part of the norm kernel we need to evaluate matrix elements of the permutation corresponding to the exchange of the last two particles, in this case $\hat{P}_{23}$. This task can be accomplished by, for example., switching to a more convenient coupling of the three-nucleon quantum numbers,

$$\left|\left[\left(n_1\ell_1 s_1 I_1 T_1; \frac{1}{2}\frac{1}{2}\right) sT; n\ell\right] J^\pi T\right\rangle = \sum_Z \hat{Z}\hat{I}_1 (-)^{\ell_1+s_1+\frac{1}{2}+s} \begin{Bmatrix} \ell_1 & s_1 & I_1 \\ \frac{1}{2} & s & Z \end{Bmatrix} \times \sum_\Lambda \hat{\Lambda}\hat{s}(-)^{Z+\ell+s+\Lambda} \begin{Bmatrix} Z & \ell_1 & s \\ \ell & J & \Lambda \end{Bmatrix} \times \left|\left[(n_1\ell_1, n\ell)\Lambda; \left(s_1\frac{1}{2}\right) Z\right] J^\pi\right\rangle \left|\left(T_1\frac{1}{2}\right) T\right\rangle, \quad (46)$$

and observing that, as a result of the action of $\hat{P}_{23}$, the HO state $\langle \vec{\xi}_1\vec{\eta}_2|(n_1\ell_1, n\ell)\Lambda\rangle$ is changed into $\langle \vec{\xi}_1'\vec{\eta}_2'|(n_1\ell_1, n\ell)\Lambda\rangle$. The new set of Jacobi coordinates $\vec{\xi}_1'$ and $\vec{\eta}_2'$ (obtained from $\vec{\xi}_1$ and $\vec{\eta}_2$, respectively, by exchanging the single-nucleon indexes 2 and 3) can be expressed as an orthogonal transformation of the unprimed ones. Consequently, the HO states depending on them are related by the orthogonal transformation

$$\langle \vec{\xi}_1'\vec{\eta}_2'|(n_1\ell_1, n\ell)\Lambda\rangle = \sum_{NL,\mathcal{N}_1\mathcal{L}_1} (-)^{L+\mathcal{L}_1-\Lambda} \langle NL, \mathcal{N}_1\mathcal{L}_1, \Lambda | n_1\ell_1, n\ell, \Lambda\rangle_3 \times \langle \vec{\xi}_1\vec{\eta}_2|(\mathcal{N}_1\mathcal{L}_1, NL)\Lambda\rangle, \quad (47)$$

where the elements of the transformation are the general HO brackets for two particles with mass ratio $d = 3$.

After taking care of the action of $\hat{P}_{23}$ also on the spin and isospin states, one can complete the derivation and write the following expression for the $A = 3$ exchange part of the norm kernel in the SNP basis:

$$\begin{aligned}\mathcal{N}^{\rm ex}_{\nu'\nu}(r', r) = -2 \sum_{n'n} R_{n'\ell'}(r') R_{n\ell}(r) &\times \sum_{n_1'\ell_1's_1'} \langle n_1'\ell_1's_1' I_1' T_1' | 2\,\alpha_1' I_1'^{\pi_1'} T_1'\rangle \\ &\times \sum_{n_1\ell_1 s_1} \langle n_1\ell_1 s_1 I_1 T_1 | 2\,\alpha_1 I_1^{\pi_1} T_1\rangle \\ &\times \hat{T}_1'\hat{T}_1 (-)^{T_1'+T_1} \begin{Bmatrix} \frac{1}{2} & \frac{1}{2} & T_1 \\ \frac{1}{2} & T & T_1' \end{Bmatrix} \hat{s}_1'\hat{s}_1\hat{I}_1'\hat{I}_1\hat{s}'\hat{s}\,(-)^{\ell_1+\ell} \\ &\times \sum_{\Lambda,Z} \hat{\Lambda}^2\hat{Z}^2 (-)^\Lambda \begin{Bmatrix} \frac{1}{2} & \frac{1}{2} & s_1 \\ \frac{1}{2} & Z & s_1' \end{Bmatrix} \begin{Bmatrix} \ell_1' & Z & s' \\ J & \ell' & \Lambda \end{Bmatrix} \\ &\times \begin{Bmatrix} \ell_1' & Z & s' \\ \frac{1}{2} & I_1' & s_1' \end{Bmatrix} \begin{Bmatrix} \ell_1 & Z & s \\ J & \ell & \Lambda \end{Bmatrix} \begin{Bmatrix} \ell_1 & Z & s \\ \frac{1}{2} & I_1 & s_1 \end{Bmatrix} \\ &\times \langle n'\ell', n_1'\ell_1', \Lambda | n_1\ell_1, n\ell, \Lambda\rangle_3. \end{aligned} \quad (48)$$

Here we recall that the index ν stands for the collection of quantum numbers $\{A-1\ \alpha_1 I_1^{\pi_1} T_1;\ 1\frac{1}{2}\frac{1}{2};\ s\ell\}$, whereas ν' is an analogous index containing the primed quantum numbers.

The derivation of "direct" and "exchange" potential kernels, although complicated by the need for additional orthogonal transformations and the presence of the two-body matrix elements of the interaction, proceeds along the same lines presented here (see Appendix A1). As a final remark, we note that the exchange part of the norm kernel [Eq. (48)] and the direct potential kernel [Eq. (A4)] are symmetric under exchange of prime and unprimed indexes, and primed and unprimed coordinates, whereas the same is not true of the exchange part of the potential kernel [Eq. (A5)]. Indeed, as anticipated in Sec. II D, the Hamiltonian kernel defined in Eq. (38) is explicitly non-Hermitian.

2. *Single-particle Slater-determinant derivation*

The matrix elements of the operators $\hat{P}_{A-1,A}$, $V_{A-1,A}(1-\hat{P}_{A-1,A})$, and $\hat{P}_{A-1,A}V_{A-2,A-1}$ can be more intuitively derived by working within the SD basis of Eq. (24). Using the second-quantization formalism, they can be related to linear combinations of matrix elements of creation and annihilation operators between $(A-1)$-nucleon SD states. These quantities can be easily calculated by shell-model codes. Here we outline the main stages of the derivation.

The SD basis [Eq. (24)] simplifies in the case of a single-nucleon projectile to

$$\begin{aligned}\left|\Phi_{\nu n}^{J^\pi T}\right\rangle_{\rm SD} &= \left[\left(|A-1\ \alpha_1 I_1 T_1\rangle_{\rm SD}\left|1\,\frac{1}{2}\frac{1}{2}\right\rangle\right)^{(sT)} Y_\ell(\hat{r}_A)\right]^{(J^\pi T)} R_{n\ell}(r_A)\\ &= \sum_j (-1)^{I_1+J+j}\begin{Bmatrix} I_1 & \frac{1}{2} & s\\ \ell & J & j\end{Bmatrix}\hat{s}\,\hat{j}\\ &\quad\times\left[|A-1\ \alpha_1 I_1 T_1\rangle_{\rm SD}\ \varphi_{n\ell j\frac{1}{2}}(\vec{r}_A\sigma_A\tau_A)\right]^{(J^\pi T)},\end{aligned}\tag{49}$$

with $\nu=\{A-1\ \alpha_1 I_1^{\pi_1} T_1; 1\frac{1}{2}\frac{1}{2}; s\ell\}$ and the HO single-particle wave function $\varphi_{n\ell jm\frac{1}{2}m_t}(\vec{r}_A\sigma_A\tau_A)=R_{n\ell}(r_A)\left(Y_\ell(\hat{r}_A)\chi_{\frac{1}{2}}(\sigma_A)\right)^{(j)}_m\chi_{\frac{1}{2}m_t}(\tau_A)$. To obtain the exchange part of the norm kernel [Eq. (37)] we first calculate the permutation operator matrix elements within the basis of Eq. (49). By expressing the position state of the nucleon $(A-1)$ as $|\vec{r}_{A-1}\sigma_{A-1}\tau_{A-1}\rangle=\sum_{n\ell jm\frac{1}{2}m_t}\varphi^*_{n\ell jm\frac{1}{2}m_t}(\vec{r}_{A-1}\sigma_{A-1}\tau_{A-1})\,a^\dagger_{n\ell jm\frac{1}{2}m_t}|0\rangle$ we arrive at

$$\begin{aligned}{}_{\rm SD}\left\langle\Phi_{\nu' n'}^{J^\pi T}\right|\hat{P}_{A,A-1}\left|\Phi_{\nu n}^{J^\pi T}\right\rangle_{\rm SD} &= \frac{1}{A-1}\sum_{jj'K\tau}\hat{s}\hat{s}'\hat{j}\hat{j}'\hat{K}\hat{\tau}(-1)^{I_1'+j'+J}(-1)^{T_1+\frac{1}{2}+T}\begin{Bmatrix} I_1 & \frac{1}{2} & s\\ \ell & J & j\end{Bmatrix}\begin{Bmatrix} I_1' & \frac{1}{2} & s'\\ \ell' & J & j'\end{Bmatrix}\begin{Bmatrix} I_1 & K & I_1'\\ j' & J & j\end{Bmatrix}\begin{Bmatrix} T_1 & \tau & T_1'\\ \frac{1}{2} & T & \frac{1}{2}\end{Bmatrix}\\ &\quad\times{}_{\rm SD}\left\langle A-1\ \alpha_1' I_1' T_1'\right|\left|\left|\left(a^\dagger_{n\ell j\frac{1}{2}}\tilde{a}_{n'\ell' j'\frac{1}{2}}\right)^{(K\tau)}\right|\right|\left|A-1\,\alpha_1\ I_1 T_1\right\rangle_{\rm SD}.\end{aligned}\tag{50}$$

Here, ${}_{\rm SD}\langle A-1\,\alpha_1'\ I_1' T_1'||\left|(a^\dagger_{n\ell j\frac{1}{2}}\tilde{a}_{n'\ell' j'\frac{1}{2}})^{(K\tau)}\right||A-1\ \alpha_1\ I_1 T_1\rangle_{\rm SD}$ are one-body density matrix elements (OBDME) of the target nucleus and $\tilde{a}_{n'\ell' j' m'\frac{1}{2}m_t'}=(-1)^{j'-m'+\frac{1}{2}-m_t'}\ a_{n'\ell' j'-m'\frac{1}{2}-m_t'}$. Next we extract the corresponding translationally invariant matrix elements, $\langle\Phi^{(A-1,1)J_r^{\pi_r}T}_{\nu_r' n_r'}|\hat{P}_{A,A-1}|\Phi^{(A-1,1)J_r^{\pi_r}T}_{\nu_r n_r}\rangle$, by inverting Eq. (32) for $a=1$ and $\hat{\mathcal{O}}_{\rm t.i.}=\hat{P}_{A-1,A}$. The final step follows easily from Eq. (37).

The same procedure is applied also for calculating "direct" and "exchange" potential kernels. In this case the transition matrix elements on the SD basis are, respectively,

$$\begin{aligned}&{}_{\rm SD}\left\langle\Phi_{\nu' n'}^{J^\pi T}\right|V_{A-1,A}(1-\hat{P}_{A,A-1})\left|\Phi_{\nu n}^{J^\pi T}\right\rangle_{\rm SD}\\ &= \frac{1}{A-1}\sum_{jj'K\tau}\sum_{n_a l_a j_a}\sum_{n_b l_b j_b}\sum_{J_0 T_0}\hat{s}\hat{s}'\hat{j}\hat{j}'\hat{K}\hat{\tau}\hat{J}_0^2\hat{T}_0^2(-1)^{I_1'+j'+J}(-1)^{T_1-\frac{1}{2}+T}\begin{Bmatrix} I_1 & \frac{1}{2} & s\\ \ell & J & j\end{Bmatrix}\begin{Bmatrix} I_1' & \frac{1}{2} & s'\\ \ell' & J & j'\end{Bmatrix}\begin{Bmatrix} I_1 & K & I_1'\\ j' & J & j\end{Bmatrix}\begin{Bmatrix} j_b & j_a & K\\ j' & j & J_0\end{Bmatrix}\begin{Bmatrix} T_1 & \tau & T_1'\\ \frac{1}{2} & T & \frac{1}{2}\end{Bmatrix}\\ &\quad\times\begin{Bmatrix}\tau & \frac{1}{2} & \frac{1}{2}\\ T_0 & \frac{1}{2} & \frac{1}{2}\end{Bmatrix}\sqrt{1+\delta_{(n_a l_a j_a),(n'\ell' j')}}\sqrt{1+\delta_{(n_b l_b j_b),(n\ell j)}}\left\langle\left(n_a l_a j_a\frac{1}{2}\right)\left(n'\ell' j'\frac{1}{2}\right)J_0 T_0\right|V\left|\left(n\ell j\frac{1}{2}\right)\left(n_b l_b j_b\frac{1}{2}\right)J_0 T_0\right\rangle\\ &\quad\times{}_{\rm SD}\left\langle A-1\ \alpha_1' I_1' T_1'\right|\left|\left(a^\dagger_{n_a l_a j_a\frac{1}{2}}\tilde{a}_{n_b l_b j_b\frac{1}{2}}\right)^{(K\tau)}\right|\left|A-1\ \alpha_1 I_1 T_1\right\rangle_{\rm SD}\end{aligned}\tag{51}$$

and

$$
\begin{aligned}
&{}_{\rm SD}\langle \Phi^{J^\pi T}_{\nu' n'} | \hat{P}_{A,A-1} V_{A-2,A-1} | \Phi^{J^\pi T}_{\nu n} \rangle_{\rm SD} \\
&= \frac{1}{2(A-1)(A-2)} \sum_{jj'K\tau} \sum_{n_a l_a j_a} \sum_{n_b l_b j_b} \sum_{n_c l_c j_c} \sum_{n_d l_d j_d} \sum_{K_a \tau_a K_{cd} \tau_{cd}} \hat{s}\hat{s}'\hat{j}\hat{j}'\hat{K}\hat{\tau}\hat{K}_a\hat{\tau}_a\hat{K}_{cd}\hat{\tau}_{cd}(-1)^{I_1'+j'+J+K+j+j_a+j_c+j_d}(-1)^{T_1+\frac{1}{2}+\tau+T} \\
&\times \begin{Bmatrix} I_1 & \frac{1}{2} & s \\ \ell & J & j \end{Bmatrix} \begin{Bmatrix} I_1' & \frac{1}{2} & s' \\ \ell' & J & j' \end{Bmatrix} \begin{Bmatrix} I_1 & K & I_1' \\ j' & J & j \end{Bmatrix} \begin{Bmatrix} K_a & K_{cd} & K \\ j' & j & j_a \end{Bmatrix} \begin{Bmatrix} T_1 & \tau & T_1' \\ \frac{1}{2} & T & \frac{1}{2} \end{Bmatrix} \begin{Bmatrix} \tau & \tau_a & \tau_{cd} \\ \frac{1}{2} & \frac{1}{2} & \frac{1}{2} \end{Bmatrix} \sqrt{1+\delta_{(n_a l_a j_a),(n'\ell' j')}} \sqrt{1+\delta_{(n_c l_c j_c),(n_d l_d j_d)}} \\
&\times \left\langle \left(n'\ell' j' \frac{1}{2}\right) \left(n_a l_a j_a \frac{1}{2}\right) K_{cd}\tau_{cd} \middle| V \middle| \left(n_d l_d j_d \frac{1}{2}\right) \left(n_c l_c j_c \frac{1}{2}\right) K_{cd}\tau_{cd} \right\rangle \\
&\times {}_{\rm SD}\langle A-1\ \alpha_1' I_1' T_1' || | \left(\left(a^\dagger_{n\ell j \frac{1}{2}} a^\dagger_{n_a l_a j_a \frac{1}{2}}\right)^{(K_a\tau_a)} \left(\tilde{a}_{n_c l_c j_c \frac{1}{2}} \tilde{a}_{n_d l_d j_d \frac{1}{2}}\right)^{(K_{cd}\tau_{cd})} \right)^{(K\tau)} || | A-1\ \alpha_1 I_1 T_1 \rangle_{\rm SD}. \qquad (52)
\end{aligned}
$$

The "direct" matrix element [Eq. (51)] depends on the OBDME, whereas the "exchange" matrix element [Eq. (52)] depends on two-body density matrix elements (TBDME) of the target nucleus. This is easily understandable as the former involves only a single nucleon of the target, whereas the latter involves two nucleons of the target (see also Fig. 2). We note that the two-body matrix elements of the interaction V are evaluated by using just the first two terms of Eq. (8); that is, $V_{ij} = V_N(ij) + \frac{e^2(1+\tau_i^z)(1+\tau_j^z)}{4|\vec{r}_i - \vec{r}_j|}$ as the average Coulomb interaction is taken care of with the help of Eq. (43). We also note that, as a consistency check, it is possible to recover the Eq. (50) from either Eq. (51) or Eq. (52) by setting the NN interaction operator V to the identity opertor.

3. *Illustrative examples*

The n-α system provides a convenient ground to explore the characteristic features of the integral kernels obtained by applying the NCSM/RGM approach within the SNP formalism. Because of the tightly bound structure of ^{4}He, an expansion in n-α channel states allows us to describe fairly well the low-energy properties of the ^{5}He system. The latter (likewise ^{5}Li) is an unbound system, its ground state being a narrow P-wave resonance in the $\frac{3}{2}^-\ \frac{1}{2}$ channel.

Figures 3–7 and Table I present results of single-channel calculations carried out using n-α cluster channels with the α particle in its g.s. (Note that throughout this section the index $\nu = \{4\,\text{g.s.}\ 0^+0; 1\,\frac{1}{2}^+\frac{1}{2}; \frac{1}{2}\ell\}$ can and will be simply replaced by the quantum number ℓ.) The interaction models adopted are the next-to-next-to-next-to-leading order (N^{3}LO) NN potential [32] derived within chiral effective-field theory (χEFT) at the N^{3}LO and the $V_{\text{low}\,k}$ NN potential [33] derived from AV18 with cutoff $\Lambda = 2.1$ fm^{-1}. Although χEFT forces are known to present a relatively soft core, the large but finite model spaces computationally achievable are still insufficient to reach a full convergence through a "bare" calculation. Therefore, for this potential we utilize two-body effective interactions tailored to the truncated model spaces as outlined in Sec. II B. Results for the $V_{\text{low}\,k}$ potential are obtained using the "bare" interaction.

The overall convergence behavior of the integral kernels is influenced by both the convergence of the eigenstates entering the binary-cluster basis, in the specific case the ^{4}He g.s., and the convergence of the radial expansion of Eq. (21). As an example, Fig. 3 presents the behavior of the exchange part of the norm kernel with respect to the increase of the model-space size obtained for the $J^\pi T = \frac{1}{2}^+\frac{1}{2}$ and $\frac{3}{2}^-\frac{1}{2}$ five-nucleon channels, using the N^{3}LO potential.

TABLE I. The three largest negative eigenvalues of the "exchange" part of the norm kernel [Eq. (37)] for the n-^{4}He(g.s.) $J^\pi T = \frac{1}{2}^+\frac{1}{2}$ channel. Convergence is with respect to the model-space size $N_{\max}$ of the NCSM/RGM results obtained using the $V_{\text{low}\,k}$ [33] and N^{3}LO NN potentials at $\hbar\Omega = 18$ and 19 MeV, respectively. The calculated values for the AV14 NN potential of Ref. [35] are multiplied by -1 to adhere to the definition of the norm kernel adopted in the present paper.

$N_{\max}$	γ_1	γ_2	γ_3
		$V_{\text{low}\,k}$	
9	−0.9547	−0.06609	−0.00310
11	−0.9539	−0.06600	−0.00288
13	−0.9530	−0.06616	−0.00290
15	−0.9526	−0.06617	−0.00292
17	−0.9524	−0.06616	−0.00293
		N^{3}LO	
9	−0.954	−0.0633	−0.00346
11	−0.945	−0.0641	−0.00452
13	−0.938	−0.0643	−0.00524
15	−0.933	−0.0646	−0.00599
17	−0.929	−0.0645	−0.00636
19	−0.927	−0.0644	−0.00661
21	−0.926	−0.0645	−0.00684
		AV14	
FY [35]	−0.937	−0.0663	−0.00753

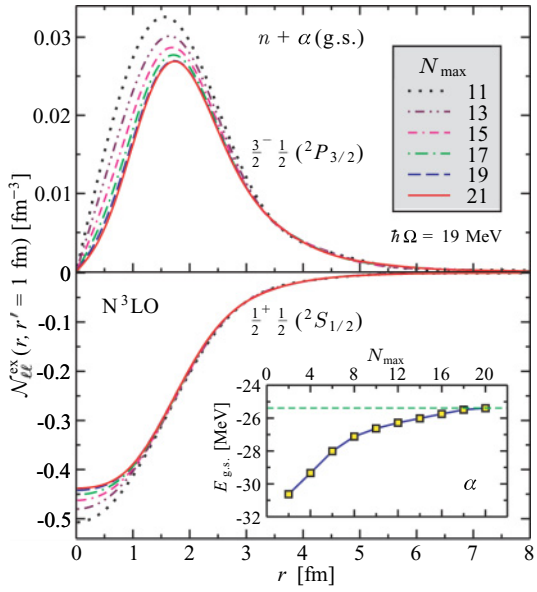

FIG. 3. (Color online) Dependence on N_{max} of the "exchange" part of the diagonal norm kernel for the n-^{4}He(g.s.) $\frac{1}{2}^+\frac{1}{2}$ ($^2S_{1/2}$), and $\frac{3}{2}^-\frac{1}{2}$ ($^2P_{3/2}$) channels as a function of the relative coordinate r at $r' = 1$ fm, using the N^{3}LO NN potential [32] at $\hbar\Omega = 19$ MeV. The inset shows the convergence pattern of the energy of the ^{4}He g.s., used to build the binary-cluster basis. The green dashed line indicates the previous NCSM evaluation of $E_{g.s.} = -25.39(1)$ MeV [34].

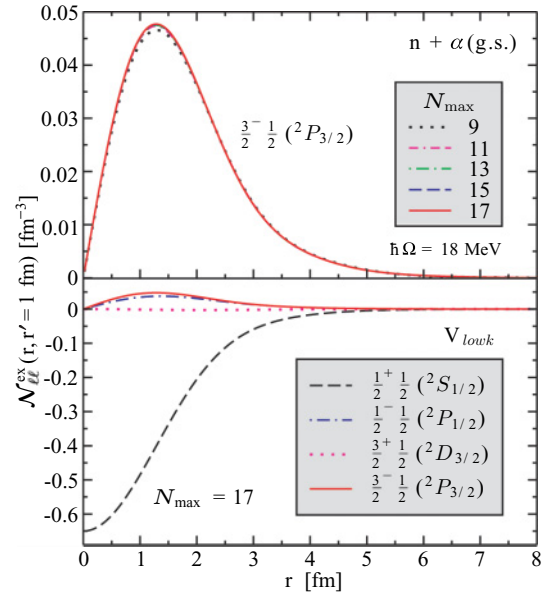

FIG. 4. (Color online) "Exchange" part of the diagonal norm kernel for the n-^{4}He(g.s.) $\frac{1}{2}^\pm\frac{1}{2}$ and $\frac{3}{2}^\mp\frac{1}{2}$ channels as a function of the relative coordinate r at $r' = 1$ fm, using the $V_{low\,k}$ NN potential [33] at $\hbar\Omega = 18$ MeV. The upper panel shows the model-space dependence of the $^2P_{3/2}$ component.

The corresponding convergence pattern for the α-particle g.s. energy is shown in the inset. To allow for the calculation of both positive- and negative-parity five-nucleon channels, for a given truncation N_{max} in the $I_1^{\pi_1}T_1 = 0^+0$ model space used to expand the g.s., a complete calculation of Eq. (37) requires an expansion over n-$\alpha J^\pi T$ states up to $N_{max} + 1$. This is the origin of the odd N_{max} values in the legend of Fig. 3 (and following). As we can see from the figure, the HO frequency $\hbar\Omega = 19$ MeV enables a quite satisfactory convergence of both ^{4}He g.s. and n-α radial expansion and hence of the integral kernel. As an example, for the $^2S_{1/2}$ channel the $N_{max} = 17$ result is already within 3% or less off the converged ($N_{max} = 21$) curve in the whole r range up to 4.5 fm. An analogous analysis of the $^2P_{3/2}$ kernels yields a somewhat larger relative difference (less than 10%) between $N_{max} = 17$ and 21 in the range between 1 and 4 fm, whereas the discrepancy increases toward the origin. In this regard, we note that the $\frac{3}{2}^-\frac{1}{2}$ kernel overall is an order of magnitude smaller than the $\frac{1}{2}^+\frac{1}{2}$ one.

The convergence rate for $V_{low\,k}$ (see upper panel of Fig. 4) is clearly much faster. Here the $^2P_{3/2}$ results for the two largest model spaces ($N_{max} = 15$ and 17) are within 0.5% or less in the whole region up to 5 fm.

Despite the mild differences in magnitude and strength distribution for small r, r' values, the $^2S_{1/2}$ and $^2P_{3/2}$ results of Figs. 3 and 4 present essentially the same shape and the same range of about 5 fm. This can be observed also in Fig. 5, which shows once again the $^2S_{1/2}$ partial wave, in terms of contour plots. (Note that the $^2S_{1/2}$ curves of Figs. 3 and 4 correspond to slices of the current plot along the $r' = 1$ fm line.) In particular, it is clear that the $^2S_{1/2}$ kernels for the two different NN potentials assume almost-identical values starting from $r, r' = 2$ fm, the N^{3}LO results being much shallower near the origin and overall less symmetric than those obtained with $V_{low\,k}$. The latter features reveal differences in the structure of the α particle obtained within the N^{3}LO and $V_{low\,k}$ NN interactions. We note that the g.s. energy and point-proton root-mean-square radius of the α particle are $-25.39(1)$ MeV and 1.515(2) fm and $-27.77(1)$ MeV and 1.4239(2) fm with the N^{3}LO and $V_{low\,k}$ potentials, respectively. In Fig. 4 (bottom panel), we compare the components of the "exchange" norm kernel up to $\ell = 2$. Contributions of higher relative angular momenta are of the same order or smaller than the $^2D_{3/2}$ partial wave. It is apparent that the $^2S_{1/2}$ channel dominates over the others and is negative. This is an effect of the Pauli exclusion principle, which forbids more than four nucleons in the s shell of a nuclear system. The four nucleons forming the ^{4}He g.s. sit mostly in the $0\hbar\Omega$ shell. Accordingly, in the $^2S_{1/2}$ channel the "exchange" part of the norm kernel suppresses the (dominant) $0\hbar\Omega$ contribution to the δ function of Eq. (35) (and, consequently, to the S-wave relative-motion wave function $g^{\frac{1}{2}^+\frac{1}{2}}_{\ell=0}$) coming from the fifth nucleon in the s-shell configuration. More precisely, the diagonalization of the "exchange" part of the norm kernel reveals the presence of an eigenvector $\mathfrak{g}^{\frac{1}{2}^+\frac{1}{2}}_{0,\Gamma}$ with eigenvalue $\gamma_\Gamma \simeq -1$ (i.e., a Pauli-forbidden state):

$$\int dr\, \mathcal{N}^{ex}_{00}(r', r)\mathfrak{g}^{\frac{1}{2}^+\frac{1}{2}}_{0,\Gamma}(r) = \gamma_\Gamma\, \mathfrak{g}^{\frac{1}{2}^+\frac{1}{2}}_{0,\Gamma}(r'). \tag{53}$$

Table I presents the three largest-negative eigenvalues for the adopted NN potentials along with their dependence upon the

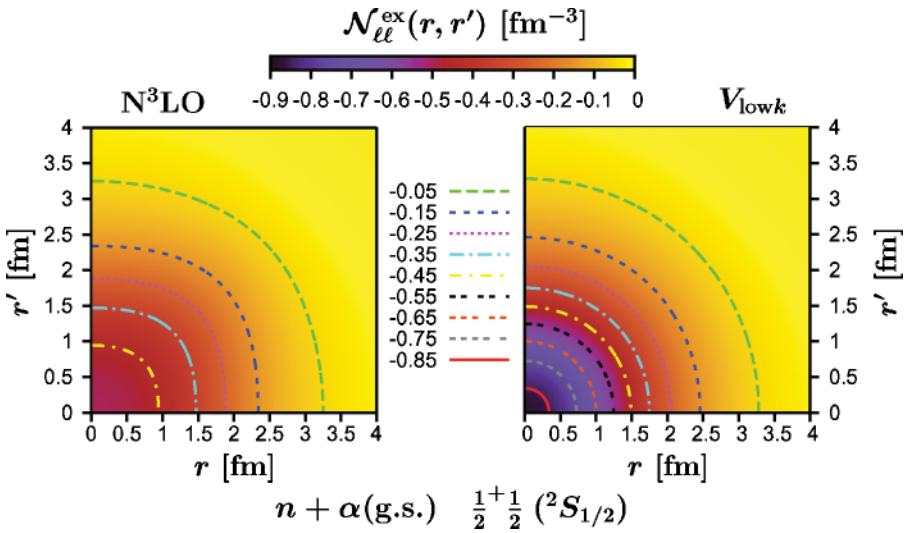

FIG. 5. (Color online) "Exchange" part of the diagonal norm kernel for the n-^{4}He(g.s.) $\frac{1}{2}^+\frac{1}{2}$ channel as a function of the relative coordinates r and r', using the N^{3}LO [32] (left) and $V_{\text{low}\,k}$ [33] (right) NN potentials at $\hbar\Omega = 19$ and 18 MeV, respectively.

model-space size. For both interactions the first eigenvalue clearly corresponds to a Pauli-forbidden state. Once again, the rate of convergence for $V_{\text{low}\,k}$ is visibly faster than for N^{3}LO, and, despite the differences noted in the integral kernels, the overall results for the eigenvalues are very close. The present results are also in good agreement (especially for N^{3}LO) with the eigenvalues obtained in Ref. [35] from a Faddeev-Yakubovsky calculation of the five-nucleon "exchange" norm, using the AV14 NN potential.

The presence of a forbidden state affects also the potential kernels. The surface plots of Figs. 6 and 7 present "direct" and "exchange" potentials for the $\frac{1}{2}^+\frac{1}{2}$ and $\frac{3}{2}^-\frac{1}{2}$ channels, respectively. In the $^2S_{1/2}$ partial wave the Pauli-exclusion principle manifests itself again in the short-range repulsive action of the "exchange" potential, which effectively suppresses the interaction between one of the nucleons inside the α particle and the fifth nucleon, both in the s-shell configuration. The situation is different in the $^2P_{3/2}$ channel, where the "exchange" kernel represents a $\sim$15% correction to the "direct" potential and generates additional attraction.

In the five-nucleon system the $\frac{1}{2}^+\frac{1}{2}$ is the only forbidden state (which is also the reason why the five-nucleon g.s. occurs in the P wave). For all other partial waves, the "exchange" part of the integral kernels introduces only a small deviation from orthogonality in the case of the norm, or small corrections to the "effective" n-α interaction, in the case of the potential. These many-body corrections induced by the nonidentical permutations in the intercluster antisymmetrizers become less and less important with increasing relative angular momentum ℓ and have a limited range of about 5 fm.

E. Orthogonalization

The appearance of the norm kernel $\mathcal{N}^{J^\pi T}_{\nu'\nu}(r',r)$ in Eq. (4) reflects the fact that the many-body wave function $\Psi^{J^\pi T}$ is expanded in terms of a nonorthogonal basis. Therefore, Eq. (4) does not represent a system of multichannel Schrödinger equations, and $g^{J^\pi T}_\nu(r)$ do not represent Schrödinger wave functions. However, as we have seen in Sec. II D 3, the nonorthogonality is short-ranged, as it originates from the nonidentical permutations in the intercluster antisymmetrizers.

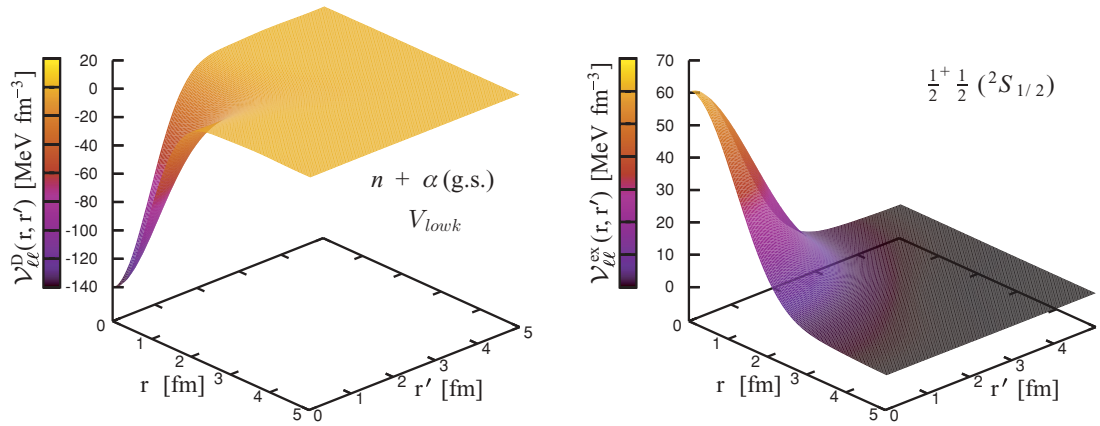

FIG. 6. (Color online) Diagonal n-^{4}He(g.s.) $\frac{1}{2}^+\frac{1}{2}$ ($^2S_{1/2}$) potential kernels as a function of the relative coordinates r and r', using the $V_{\text{low}\,k}$ [33] NN interaction. The model space and HO frequency are $N_{\max} = 17$ and $\hbar\Omega = 18$ MeV, respectively.

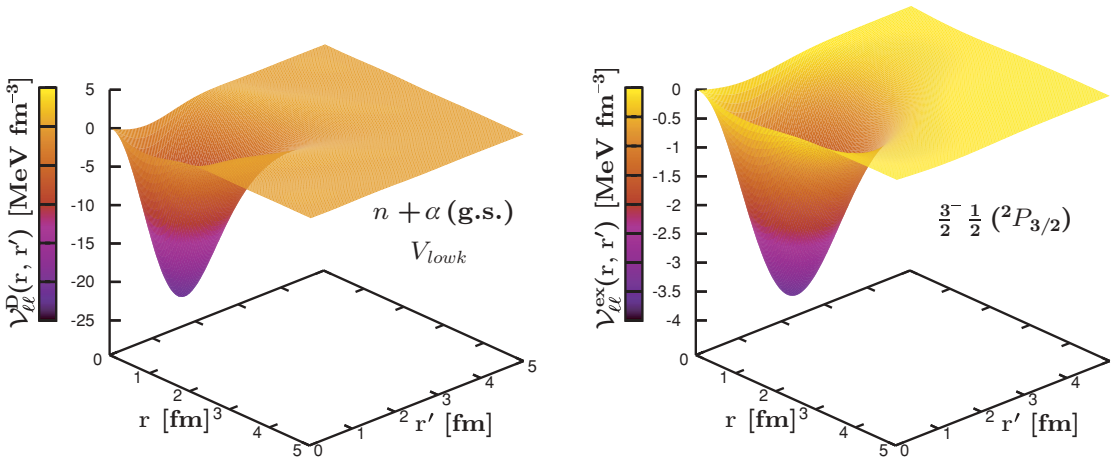

FIG. 7. (Color online) Diagonal n-^{4}He(g.s.) $\frac{3}{2}^-\frac{1}{2}$ ($^2P_{3/2}$) potential kernels as a function of the relative coordinates r and r', using the $V_{\text{low }k}$ [33] NN interaction. The model space and HO frequency are $N_{\max}=17$ and $\hbar\Omega=18$ MeV, respectively.

Thus, asymptotically one has

$$\mathcal{N}^{J^\pi T}_{\nu'\nu}(r',r)\to\delta_{\nu'\nu}\frac{\delta(r'-r)}{r'r}. \tag{54}$$

As a consequence the relative wave functions $g^{J^\pi T}_\nu(r)$ obey the same asymptotic boundary conditions as the relative wave functions in a conventional multichannel collision theory, and it is possible to define physically important quantities, such as, for example, the scattering matrix or the energy eigenvalues. The internal part of the relative wave functions, however, is still affected by the short-range nonorthogonality. Therefore, attention has to be paid when the latter wave functions are used to calculate further observables, such as, for example, radiative capture cross sections or, more in general, transition matrix elements.

Alternatively, one can introduce an orthogonalized version of Eq. (4), such as

$$\sum_\nu\int dr r^2\left[\mathbb{H}^{J^\pi T}_{\nu'\nu}(r',r)-E\delta_{\nu'\nu}\frac{\delta(r'-r)}{r'r}\right]\frac{\chi^{J^\pi T}_\nu(r)}{r}=0, \tag{55}$$

where $\mathbb{H}^{J^\pi T}_{\nu'\nu}(r',r)$ is the Hermitian energy-independent nonlocal Hamiltonian defined by

$$\mathbb{H}^{J^\pi T}_{\nu'\nu}(r',r)=\sum_{\gamma'}\int dy'y'^2\sum_\gamma\int dy\,y^2 \times\mathcal{N}^{-\frac12}_{\nu'\gamma'}(r',y')\,\bar{\mathcal{H}}^{J^\pi T}_{\gamma'\gamma}(y',y)\,\mathcal{N}^{-\frac12}_{\gamma\nu}(y,r), \tag{56}$$

and the Schrödinger wave functions $\chi^{J^\pi T}_\nu(r)$ are the new unknowns of the problem, related to $g^{J^\pi T}_\nu(r)$ through

$$\frac{\chi^{J^\pi T}_\nu(r)}{r}=\sum_\gamma\int dy\,y^2\mathcal{N}^{\frac12}_{\nu\gamma}(r,y)\,\frac{g^{J^\pi T}_\gamma(y)}{y}. \tag{57}$$

Here, $\mathcal{N}^{\frac12}_{\kappa'\kappa}(x',x)$ and $\mathcal{N}^{-\frac12}_{\kappa'\kappa}(x',x)$ represent the square root and the inverse-square root of the norm kernel, respectively. To perform these two operations, we add and subtract from the norm kernel the identity in the HO model space,

$$\mathcal{N}^{J^\pi T}_{\nu'\nu}(r',r)=\delta_{\nu'\nu}\left[\frac{\delta(r'-r)}{r'r}-\sum_n R_{n\ell}(r')R_{n\ell}(r)\right] +\sum_{n'n}R_{n'\ell'}(r')\,\Lambda^{J^\pi T}_{\nu'n',\nu n}\,R_{n\ell}(r). \tag{58}$$

The matrix $\Lambda^{J^\pi T}$ is the norm kernel within the truncated model space spanned by the HO Jacobi-channel states of Eq. (22). We give here the expression in the SNP basis [see also Eq. (37)]:

$$\Lambda^{J^\pi T}_{\nu'n',\nu n}=\delta_{\nu'\nu}\delta_{n'n}-(A-1)\langle\Phi^{J^\pi T}_{\nu'n'}|\hat{P}_{A-1,A}|\Phi^{J^\pi T}_{\nu n}\rangle. \tag{59}$$

The generalization to the case of binary clusters with $a>1$ is straightforward.

The square root and the inverse-square root of $\mathcal{N}^{J^\pi T}_{\nu'\nu}(r',r)$ are then obtained by (i) finding eigenvalues λ_Γ and eigenvectors $|\varphi^{J^\pi T}_\Gamma\rangle$ of the matrix $\Lambda^{J^\pi T}$; (ii) calculating

$$\Lambda^{\pm\frac12}_{\nu'n',\nu n}=\sum_\Gamma\langle\Phi^{J^\pi T}_{\nu'n'}|\varphi^{J^\pi T}_\Gamma\rangle\lambda^{\pm\frac12}_\Gamma\langle\varphi^{J^\pi T}_\Gamma|\Phi^{J^\pi T}_{\nu n}\rangle; \tag{60}$$

and, finally, (iii) replacing the model-space norm $\Lambda^{J^\pi T}_{\nu'n',\nu n}$ in Eq. (58) with $\Lambda^{\frac12}_{\nu'n',\nu n}$ and $\Lambda^{-\frac12}_{\nu'n',\nu n}$, respectively, that is,

$$\mathcal{N}^{\pm\frac12}_{\nu'\nu}(r',r)=\delta_{\nu'\nu}\left[\frac{\delta(r'-r)}{r'r}-\sum_n R_{n\ell}(r')R_{n\ell}(r)\right] +\sum_{n'n}R_{n'\ell'}(r')\,\Lambda^{\pm\frac12}_{\nu'n',\nu n}\,R_{n\ell}(r). \tag{61}$$

For the inverse operation to be permissible in Eq. (60) one has to exclude the subspace of (fully) Pauli-forbidden states for which $\lambda_\Gamma=0$. (We note here that in the example of Sec. II D3, the eigenvalues of the norm kernel in the $^2S_{1/2}$ are related via $\lambda_\Gamma=1+\gamma_\Gamma$.)

Both systems of coupled differential equations [Eqs. (4) and (55)] can be cast in the form

$$\left[\hat{T}_{\rm rel}(r') + \bar{V}_C(r') - \left(E - E_{\alpha'_1}^{I_1^{\pi'_1} T'_1}\right)\right] \frac{u_{\nu'}^{J^\pi T}(r')}{r'} + \sum_\nu \int dr\, r^2\, W_{\nu'\nu}^{J^\pi T}(r', r) \frac{u_\nu^{J^\pi T}(r)}{r} = 0, \qquad (62)$$

where $u_\nu^{J^\pi T}(r)$ stands for either $g_\nu^{J^\pi T}(r)$ (in the nonorthogonalized case) or $\chi_\nu^{J^\pi T}(r)$ (in the orthogonalized case), and $W_{\nu'\nu}^{J^\pi T}(r', r)$ is the potential collecting all nonlocal terms present in the original equation. Obviously, in the (nonorthogonalized) case of Eq. (4) this nonlocal potential depends upon the energy.

To provide some illustrative examples of nonlocal potentials corresponding to the orthogonalized case of Eq. (55), we turn again to the n-α system, for which, as in Sec. II D3, we will present here results of single-channel calculations with the α particle in its g.s. Figure 8 shows the three partial waves $^2S_{1/2}$, $^2P_{1/2}$, and $^2P_{3/2}$ obtained using the N^{3}LO NN potential [32]. The nonlocal potentials for the three different spin-parity channels all rapidly vanish to zero beyond about 5 fm (as already observed in the nonorthogonalized integral kernels), while presenting substantially diverse structures at short range. We note in particular the strong repulsion between nucleon and α particle induced by the Pauli-exclusion principle in the $\frac{1}{2}^+\frac{1}{2}$ channel and the potential well leading to the ^{5}He resonance in the $\frac{3}{2}^-\frac{1}{2}$ channel.

F. Solution of the radial equation

In solving Eq. (62) we assume that $\bar{V}_C(r)$ is the only interaction experienced by the clusters beyond a finite separation r_0, thus dividing the configuration space into an internal region and an external region. The radial wave function in the external region is approximated by its asymptotic form for large r,

$$u_\nu^{J^\pi T}(r) = \frac{\rm i}{2} v_\nu^{-1/2} \left[\delta_{\nu i} H_\ell^-(\eta_\nu, \kappa_\nu r) - S_{\nu i}^{J^\pi T} H_\ell^+(\eta_\nu, \kappa_\nu r)\right], \qquad (63)$$

for scattering states, or

$$u_\nu^{J^\pi T}(r) = C_\nu^{J^\pi T}\, W_\ell(\eta_\nu, \kappa_\nu r), \qquad (64)$$

for bound states. Here $H_\ell^\mp(\eta_\nu, \kappa_\nu r) = G_\ell(\eta_\nu, \kappa_\nu r) \mp {\rm i} F_\ell(\eta_\nu, \kappa_\nu r)$ are incoming and outgoing Coulomb functions, whereas $W_\ell(\eta_\nu, \kappa_\nu r)$ are Whittaker functions. They depend on the channel state relative angular momentum ℓ, wave number κ_ν, and Sommerfeld parameter η_ν. The corresponding velocity is denoted as v_ν. The scattering matrix $S_{\nu i}^{J^\pi T}$ (i being the initial channel) in Eq. (63), or binding energy and asymptotic normalization constant $C_\nu^{J^\pi T}$ in Eq. (64), together with the radial wave function in the internal region are obtained by applying to Eq. (4) or to Eq. (55) the coupled-channel R-matrix method on a Lagrange mesh [36]. For the bound-state calculation κ_ν depends on the studied binding energy. Therefore, the determination of the bound-state energy is achieved iteratively starting from an initial guess for the value of the logarithmic derivative of the wave function at the matching radius r_0.

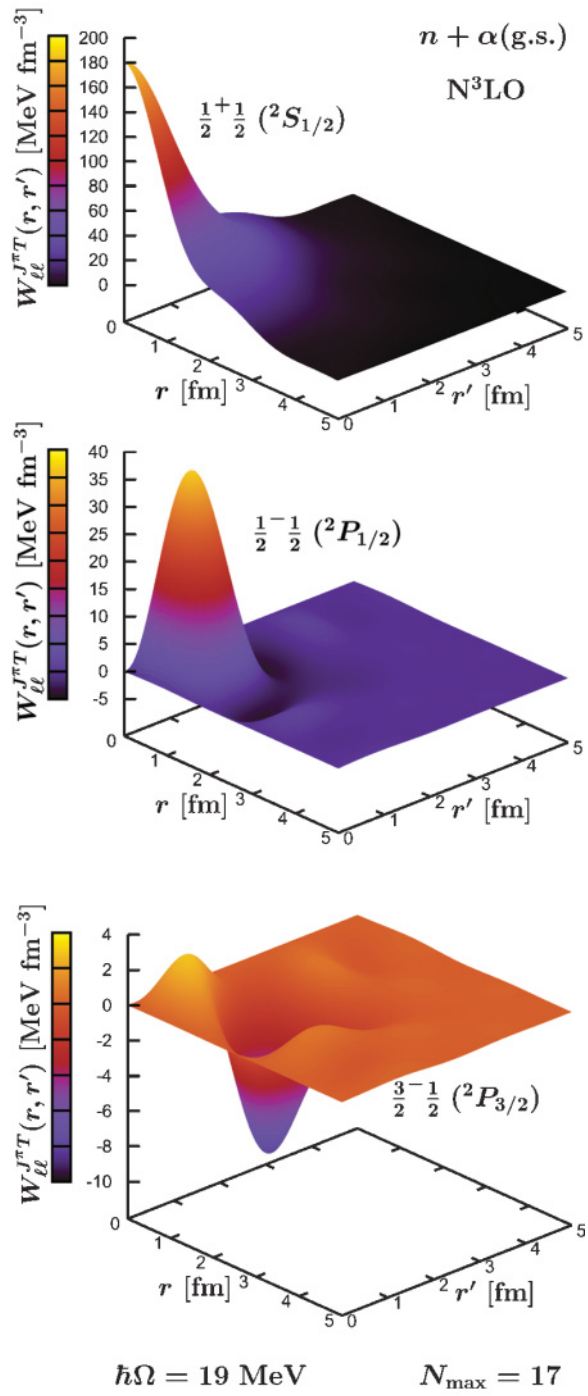

FIG. 8. (Color online) Orthogonalized nonlocal potentials for the n-α(g.s.) $J^\pi T = \frac{1}{2}^+\frac{1}{2}, \frac{1}{2}^-\frac{1}{2}$, and $\frac{3}{2}^-\frac{1}{2}$ channels as functions of the relative coordinates r and r', using the N^{3}LO NN potential [32]. The index $\nu = \{4\,{\rm g.s.}\ 0^+0; 1\,\frac{1}{2}^+\frac{1}{2}; \frac{1}{2}\ell\}$ is replaced by the quantum number ℓ for simplicity.

Finally, the accuracy of the R-matrix method on a Lagrange mesh is such that for a matching radius of $r_0 = 15$ fm, $N = 25$ mesh points are usually enough to determine a phase shift within the sixth significant digit. The typical matching radius

TABLE II. Calculated ^{3}H g.s. energy (in MeV) and n-^{3}H phase shifts (in degrees) and total cross section (in barns) for increasing $N_{\max}$ at $\hbar\Omega = 18$ MeV, obtained using the $V_{\text{low }k}$ NN potential [33]. The scattering results were obtained in a coupled-channel calculation including only the g.s. of the ^{3}H nucleus (i.e., the channels $\nu = \{3\,\text{g.s.}\ \frac{1}{2}^+\frac{1}{2};\ 1\,\frac{1}{2}^+\frac{1}{2};\ s\ \ell\}$).

$N_{\max}$	^{3}H	n-^{3}H ($E_{\text{kin}} = 0.40$ MeV)							
	$E_{\text{g.s.}}$	$0^+(^1S_0)$	$0^-(^3P_0)$	$1^+(^3S_1)$	$1^-(^1P_1)$	$1^-(^3P_1)$	$1^-(\epsilon)$	$2^-(^3P_2)$	σ_t
9	−7.80	−20.2	0.93	−18.9	0.85	1.96	−18.0	3.01	0.99
11	−7.96	−22.9	0.97	−20.4	1.04	2.36	−13.0	2.58	1.15
13	−8.02	−23.7	0.87	−21.0	1.24	2.47	−9.0	2.30	1.22
15	−8.11	−24.4	1.00	−21.8	1.40	2.44	−9.1	2.41	1.31
17	−8.12	−25.1	1.06	−22.6	1.52	2.52	−10.4	2.45	1.39
19	−8.16	−25.6	1.01	−22.9	1.64	2.60	−9.7	2.37	1.43
		n-^{3}H ($E_{\text{kin}} = 0.75$ MeV)							
		$0^+(^1S_0)$	$0^-(^3P_0)$	$1^+(^3S_1)$	$1^-(^1P_1)$	$1^-(^3P_1)$	$1^-(\epsilon)$	$2^-(^3P_2)$	σ_t
9		−27.8	2.30	−26.2	2.19	4.96	−17.5	7.51	1.06
11		−31.3	2.39	−28.1	2.63	5.93	−12.7	6.42	1.20
13		−32.4	2.15	−28.8	3.10	6.17	−9.1	5.75	1.25
15		−33.2	2.45	−29.9	3.46	6.12	−9.5	6.08	1.33
17		−34.2	2.60	−30.9	3.74	6.30	−10.7	6.19	1.41
19		−34.8	2.49	−31.3	4.00	6.49	−10.1	6.02	1.44

and number of mesh points adopted for the present calculations are $r_0 = 18$ fm and $N = 40$.

III. RESULTS

A. $A = 4$

The four-nucleon scattering problem, with its complicated interplay of low-energy thresholds and resonances, represents a serious theoretical challenge, only recently addressed by means of accurate *ab initio* calculations. Important developments in the numerical solution of the four-nucleon scattering equations in momentum space [8] and in the treatment of the long-range Coulomb interaction [37] have led to very accurate *ab initio* calculations of scattering observables in the energy region below the three-body breakup threshold.

In this section we use the four-nucleon system as a testground to study the performances of our newly developed NCSM/RGM approach within the SNP basis. In particular, we present here results of coupled-channel calculations restricted to basis channel states with the three-nucleon target in its g.s. (corresponding to channel indexes of the type $\nu = \{3\,\text{g.s.}\ \frac{1}{2}^+\frac{1}{2};\ 1\,\frac{1}{2}^+\frac{1}{2};\ s\ \ell\}$). Indeed, we are interested to the energy region below the breakup threshold of the $A = 3$ target.

We start by studying the convergence of our calculations with respect to the HO model-space size ($N_{\max}$) for the simplest of the $A = 4$ scattering channels (i.e., the n-^{3}H). This is a purely $T = 1$ system, with no Coulomb interaction between target and projectile. As the overall convergence behavior strongly depends on the model of NN interaction adopted, we first consider results obtained using the "bare" $V_{\text{low }k}$ potential [33]. These are summarized in Table II. Both ^{3}H g.s. energy and n-^{3}H scattering data present a rather weak dependence on $N_{\max}$. However, a sudden worsening in convergence rate is noticeable in the higher model spaces, especially for the phase shifts of small magnitude. This is in part a reflection of the sharp cutoff function used to derive the $V_{\text{low }k}$ potential (where here we use the version derived from AV18 with cutoff $\Lambda = 2.1$ fm^{-1}).

Next we present n-^{3}H phase shifts obtained using the N^{3}LO NN interaction [32]. The convergence behavior shown in Fig. 9 was achieved using two-body effective interactions tailored to the model-space truncation, as outlined in Sec. II B. For the $^1S_0$, $^1P_1$, and $^3S_1$ partial waves, the increase in model-space size produces gradually smaller deviations with a clear convergence toward the $N_{\max} = 19$ results. The rest of the phase shifts, particularly the $^3P_0$, show a more irregular pattern. Nevertheless, in the whole energy-range we find less than a 2° absolute difference between the phases obtained in the largest and next-to-largest model spaces. The agreement within 1.5° of the $N_{\max} = 19$ results obtained with two different HO frequencies, $\hbar\Omega = 19$ and $\hbar\Omega = 22$ MeV (see Fig. 10), is a further indication of the fairly good degree of convergence of our calculation.

To verify our approach, in Fig. 10 we compare our n-^{3}H results to earlier *ab initio* calculations performed in the framework of the AGS equations [8,38], using the same N^{3}LO NN potential. We note that in general the agreement between the two calculations worsens as the relative kinetic energy in the c.m. frame, E_{kin}, increases. For the P waves in particular we can reasonably reproduce the AGS calculation for energies within 1 MeV whereas we can find differences as large as 17°($^3P_2$) at $E_{\text{kin}} = 2.6$ MeV. In Fig. 11 an analogous comparison performed for a second realistic NN interaction, the CD-Bonn potential [39], leads to a similar picture. (Note that, as for N^{3}LO, the NCSM/RGM results for CD-Bonn were also obtained by using two-body effective interactions.) These discrepancies are due to the influence, increasing with energy,

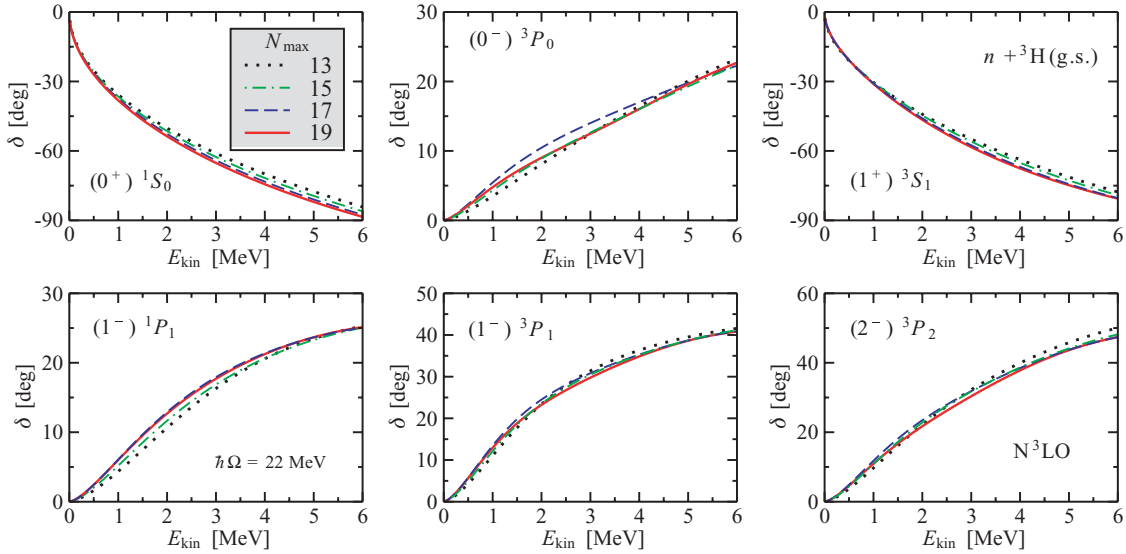

FIG. 9. (Color online) Calculated n-^{3}H phase shifts as a function of the relative kinetic energy in the c.m. frame, E_{kin}, using the N^{3}LO NN potential [32] in the model spaces $N_{max} = 11$–19, at $\hbar\Omega = 22$ MeV. All results were obtained in a coupled-channel calculation including only the g.s. of the ^{3}H nucleus (i.e., the channels $\nu = \{3\,\text{g.s.}\ \frac{1}{2}^+\frac{1}{2};\ 1\,\frac{1}{2}^+\frac{1}{2};\ s\,\ell\}$).

played by closed channels not included in our calculations, such as those with the $A-1=3$ eigenstates above the $I_1^{\pi_1} = \frac{1}{2}^+$ g.s. and $(A-a=2, a=2)$ configurations, present in the AGS results. As an indication, in Ref. [8] it was shown that the omission of three-nucleon partial waves with $\frac{1}{2} < I_1 \leqslant \frac{5}{2}$ leads to effects of comparable magnitude on the AGS results, especially for the $^3S_1$, $^3P_1$, and $^3P_2$.

All $A-1=3$ states but the $I_1^{\pi_1} = \frac{1}{2}^+$ g.s. are in the continuum and correspond to a breakup of the three-nucleon target. Therefore, the corresponding $(A-a=3, a=1)$ channels do not represent "open" rearrangement channels in the energy range considered here. However, it is clear from the previous analysis that the virtual excitation of the $A-1=3$ target has an important influence on the n-^{3}H elastic phase shifts and should be included in the NCSM/RGM approach to reach full convergence, and hence agreement with the AGS calculation. Obviously, considering the localized nature of the NCSM wave functions, for each $I_1^{\pi_1} \neq \frac{1}{2}^+$ one obtains a large series of positive-energy eigenstates corresponding to a denser and denser discretization of the $A-1=3$ continuum, as the HO model space increases. Consequently, it would not be conceptually sound to try and include these states in the NCSM/RGM SNP basis, nor would it be computationally feasible. However, the $A=4$ low-lying spectrum contains a finite number of fairly narrow resonances, which can be reasonably reproduced by diagonalizing the four-body

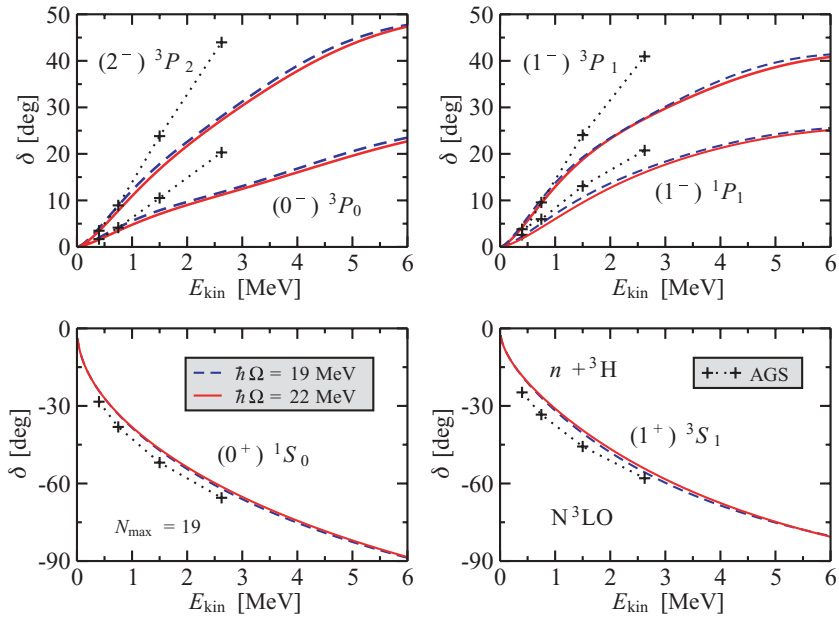

FIG. 10. (Color online) Calculated n-^{3}H phase shifts using the N^{3}LO NN potential [32] for $N_{max} = 19$ and $\hbar\Omega = 19$ and 22 MeV, compared to AGS results of Refs. [8,38]. All NCSM/RGM results were obtained in a coupled-channel calculation including only the g.s. of the ^{3}H nucleus (i.e., the channels $\nu = \{3\,\text{g.s.}\ \frac{1}{2}^+\frac{1}{2};\ 1\,\frac{1}{2}^+\frac{1}{2};\ s\,\ell\}$).

TABLE III. Calculated ^{3}He g.s. energy (in MeV) and p-^{3}He phase shifts (in degrees) for increasing $N_{\max}$ at $\hbar\Omega = 18$ MeV, obtained using the $V_{\text{low }k}$ NN potential [33]. The scattering results were obtained in a coupled-channel calculation including only the g.s. of the ^{3}He nucleus (i.e., the channels $\nu = \{3\,\text{g.s.}\ \frac{1}{2}^+\frac{1}{2};\ 1\frac{1}{2}^+\frac{1}{2};\ s\ \ell\}$).

$N_{\max}$	^{3}He	p-^{3}He ($E_{\text{kin}} = 0.40$ MeV)						
	$E_{\text{g.s.}}$	$0^+(^1S_0)$	$0^-(^3P_0)$	$1^+(^3S_1)$	$1^-(^1P_1)$	$1^-(^3P_1)$	$1^-(\epsilon)$	$2^-(^3P_2)$
9	−7.05	−5.88	0.304	−5.88	0.264	0.59	−17.7	0.884
11	−7.22	−7.71	0.350	−6.48	0.350	0.74	−12.8	0.808
13	−7.29	−7.72	0.364	−6.61	0.460	0.83	−8.7	0.778
15	−7.37	−8.15	0.449	−6.87	0.561	0.87	−8.2	0.851
17	−7.39	−8.24	0.525	−7.11	0.662	0.96	−9.8	0.926
19	−7.42	−8.48	0.554	−7.08	0.758	1.04	−8.9	0.950
		p-^{3}He ($E_{\text{kin}} = 0.75$ MeV)						
		$0^+(^1S_0)$	$0^-(^3P_0)$	$1^+(^3S_1)$	$1^-(^1P_1)$	$1^-(^3P_1)$	$1^-(\epsilon)$	$2^-(^3P_2)$
9		−12.6	1.14	−12.5	1.04	2.29	−17.2	3.38
11		−15.9	1.30	−13.6	1.35	2.83	−12.5	3.05
13		−16.0	1.34	−13.9	1.73	3.15	−8.6	2.93
15		−16.8	1.63	−14.4	2.07	3.28	−8.4	3.20
17		−17.0	1.87	−14.9	2.41	3.56	−10.0	3.46
19		−17.4	1.95	−14.9	2.71	3.83	−9.16	3.51

Hamiltonian in the NCSM model space. Therefore, it is clear that the most efficient way of tackling the $A = 4$ scattering problem would be for us to use an over-complete model space formed by both traditional NCSM four-body states and NCSM/RGM cluster states. Although it is in our intention to pursue this approach, we leave it for future investigation.

In the remaining part of this section we will discuss the scattering of protons on ^{3}He targets. This is once again a purely $T = 1$ system, but it differs from the n-^{3}H case because of the presence of the Coulomb interaction between the clusters, both of which are charged. The treatment of the Coulomb interaction between target and projectile, as explained in Sec. II, does not represent a major obstacle in the NCSM/RGM approach. In particular, in the following we will show that the p-^{3}He phase shifts present a similar convergence trend as the one observed in their neutral counterparts.

To perform a direct comparison with the n-^{3}H data, in Table III we present ^{3}He g.s. energy and p-^{3}He scattering phase shifts for the same ("bare") $V_{\text{low }k}$ NN potential [33] and relative kinetic-energy values as in Table II. As expected, the growth of the nuclear phase shifts from zero energy is slower in the presence of the Coulomb repulsion between the clusters. This is especially visible at the very low energies considered here ($E_{\text{kin}} = 0.4$ and 0.75 MeV). As the scattering data, particularly in the P waves, are very small in magnitude, the somewhat slower convergence rate in the biggest model

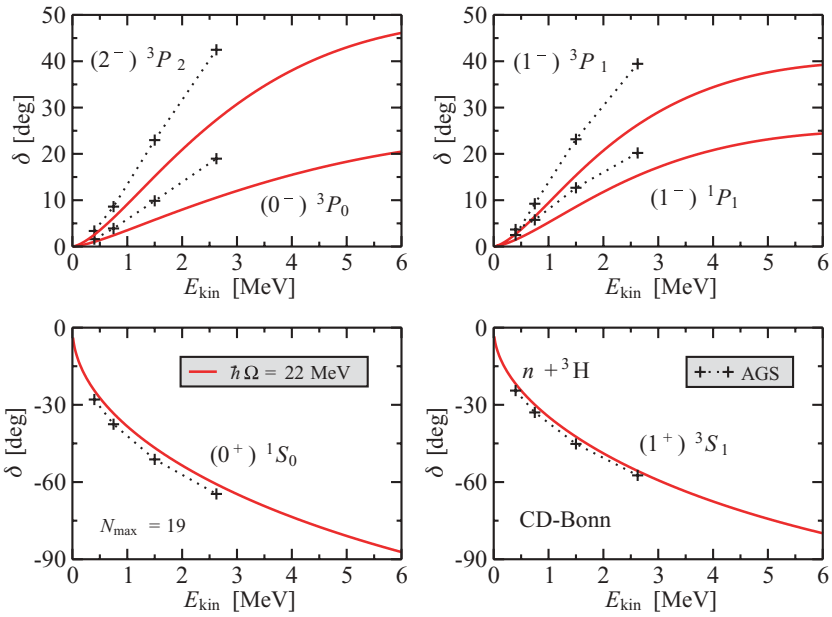

FIG. 11. (Color online) Calculated n-^{3}H phase shifts using the CD-Bonn NN potential [39] for $N_{\max} = 19$ and $\hbar\Omega = 19$ MeV, compared to AGS results of Refs. [8,38]. All NCSM/RGM results were obtained in a coupled-channel calculation including only the g.s. of the ^{3}H nucleus (i.e., the channels $\nu = \{3\,\text{g.s.}\ \frac{1}{2}^+\frac{1}{2};\ 1\frac{1}{2}^+\frac{1}{2};\ s\ \ell\}$).

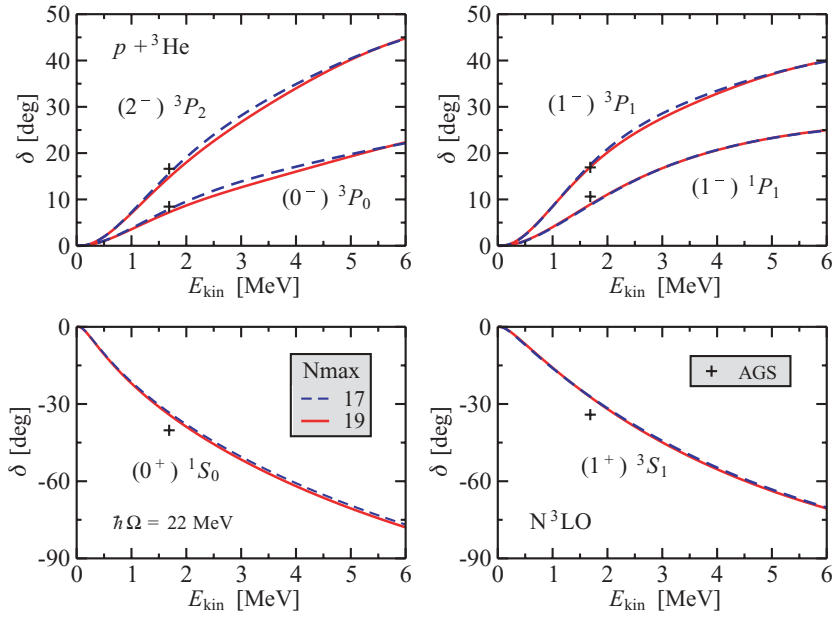

FIG. 12. (Color online) Calculated p-^{3}He phase shifts for the N^{3}LO NN potential [32] in the model spaces $N_{\max} = 17$–19, at $\hbar\Omega = 22$ MeV, compared to AGS results of Ref. [38]. All NCSM/RGM results were obtained in a coupled-channel calculation including only the g.s. of the ^{3}He nucleus (i.e., the channels $\nu = \{3\,\text{g.s.}\ \frac{1}{2}^+\frac{1}{2};\ 1\,\frac{1}{2}^+\frac{1}{2};\ s\,\ell\}$).

spaces already noticed in the n-^{3}H case is emphasized even more here. This feature, partly related to the sharp cutoff of the $V_{\text{low}\,k}$ potential, results in differences of a few tenths of a degree between the $N_{\max} = 17$ and $N_{\max} = 19$ phase shifts.

Figure 12 shows the results of this work (solid and dashed lines) along with those of AGS calculations [38] (+ symbols) for the p-^{3}He phase shifts obtained using the N^{3}LO NN potential. The use of two-body effective interactions tailored to the size of the adopted model spaces guarantees also in this case a fairly good agreement (of the same order as in Fig. 9) between the $N_{\max} = 17$ and $N_{\max} = 19$ calculations. The comparison to the AGS results shows that the NCSM/RGM SNP basis with the ^{3}He nucleus in its g.s. provides the bulk of the p-^{3}He elastic phase shifts, confirming the observations made for the n-^{3}H scattering.

B. $A = 5$

Driven by wider efforts to develop a predictive *ab initio* theory of low-energy reactions on light nuclei, *ab initio* calculations for scattering processes involving five nucleons are beginning to be realized in the past couple of years, but they are still a rare exception. First, the n-α low-lying $J^\pi = 3/2^-$ and $1/2^-$ P-wave resonances as well as the $1/2^+$ S-wave nonresonant scattering below 5 MeV c.m. energy were obtained using the AV18 NN potential with and without the three-nucleon force, chosen to be either the Urbana IX or the Illinois-2 model [9]. The results of these Green's function Monte Carlo (GFMC) calculations revealed sensitivity to the internucleon interaction, and in particular to the strength of the spin-orbit force. Soon after, the development of the *ab initio* NCSM/RGM approach allowed us to calculate both n-α and (for the first time) p-α scattering phase shifts for energies up to the inelastic threshold, using realistic NN potentials [17]. Indeed, nucleon-α scattering provides one of the best-case scenario for the application of the NCSM/RGM approach within the SNP basis. This process is characterized by a single open channel up to the ^{4}He breakup threshold, which is fairly high in energy. In addition, the low-lying resonances of the ^{4}He nucleus are narrow enough to be reasonably reproduced by diagonalizing the four-body Hamiltonian in the NCSM model space. Therefore, they can be consistently included as closed channels in the NCSM/RGM SNP model space. In the following we give a detailed description of previously published [17] and new results for nucleon-α scattering.

First we present single-channel calculations carried out using n-α channel states with the α particle in its g.s., that is, characterized by the channel index $\nu = \{4\,\text{g.s.}\ 0^+0;\ 1\,\frac{1}{2}^+\frac{1}{2};\ \frac{1}{2}\ell\}$ (or simply by the angular quantum number ℓ). In particular, Table IV shows the good degree of convergence with respect

TABLE IV. Calculated ^{4}He g.s. energy (in MeV) and n-^{4}He phase shifts (in degrees) and total cross sections (in barns) for increasing $N_{\max}$ at $\hbar\Omega = 18$ MeV, obtained using the $V_{\text{low}\,k}$ NN potential [33]. The scattering results were obtained in a single-channel calculation including only the g.s. of the ^{4}He nucleus (i.e., the channel $\nu = \{4\,\text{g.s.}\ 0^+0;\ 1\,\frac{1}{2}^+\frac{1}{2};\ \frac{1}{2}\ell\}$).

$N_{\max}$	^{4}He	n-^{4}He ($E_{\text{kin}} = 2.5$ MeV)			
	$E_{\text{g.s.}}$	$\frac{1}{2}^+(^2S_{1/2})$	$\frac{1}{2}^-(^2P_{1/2})$	$\frac{3}{2}^-(^2P_{3/2})$	σ_t
9	−27.00	−40.0	15.6	59.9	2.59
11	−27.41	−41.2	16.5	54.8	2.41
13	−27.57	−41.8	16.4	54.5	2.41
15	−27.75	−42.2	16.6	55.3	2.46
17	−27.77	−42.5	16.6	55.2	2.46
		n-^{4}He ($E_{\text{kin}} = 5.0$ MeV)			
		$\frac{1}{2}^+(^2S_{1/2})$	$\frac{1}{2}^-(^2P_{1/2})$	$\frac{3}{2}^-(^2P_{3/2})$	σ_t
9		−57.9	33.5	81.8	1.95
11		−58.6	33.7	86.1	1.98
13		−58.7	34.0	85.7	1.98
15		−58.7	33.9	84.6	1.97
17		−58.6	33.9	84.8	1.97

TABLE V. Calculated p-^{4}He phase shifts (in degrees) for increasing $N_{\max}$ at $\hbar\Omega = 18$ MeV, using the $V_{\text{low }k}$ NN potential [33]. Results were obtained in a single-channel calculation including only the g.s. of the ^{4}He nucleus (i.e., the channel $\nu = \{4\,\text{g.s.}\,0^+0;\ 1\,\frac{1}{2}^+\frac{1}{2};\ \frac{1}{2}\,\ell\}$).

$N_{\max}$	p-^{4}He ($E_{\text{kin}} = 2.5$ MeV)		
	$\frac{1}{2}^+(^2S_{1/2})$	$\frac{1}{2}^-(^2P_{1/2})$	$\frac{3}{2}^-(^2P_{3/2})$
9	−26.4	12.7	44.9
11	−27.2	14.2	38.9
13	−27.3	15.0	39.1
15	−27.2	15.7	39.9
17	−27.3	16.1	40.0
	p-^{4}He ($E_{\text{kin}} = 5.0$ MeV)		
	$\frac{1}{2}^+(^2S_{1/2})$	$\frac{1}{2}^-(^2P_{1/2})$	$\frac{3}{2}^-(^2P_{3/2})$
9	−45.8	31.3	76.5
11	−46.4	31.9	80.2
13	−46.6	32.0	80.0
15	−46.6	32.1	79.9
17	−46.5	32.0	79.9

to $N_{\max}$ obtained for the ^{4}He g.s., and for the n-α ($^2S_{1/2}$, $^2P_{1/2}$, and $^2P_{3/2}$) phase shifts and total cross section at $E_{\text{kin}} = 2.5$ and 5 MeV, using the (bare) $V_{\text{low }k}$ NN interaction.

The corresponding p-α scattering phase shifts can be found in Table V.

The HO model-space dependence of the $V_{\text{low }k}$ n-α phase shifts is presented also in the left panel of Fig. 13, where it is explored for a wider range of energies, and compared to an analogous plot for the N^{3}LO NN interaction (central panel). Despite the use of two-body effective interaction as outlined in Sec. II B, the convergence rate is visibly much slower for N^{3}LO. This gives a measure of the stronger short-range correlations generated by this potential. The $^2P_{3/2}$ phase shifts present the largest (up to 5° in the energy range between 1 and 4 MeV) differences between the $N_{\max} = 15$ and 17 calculations, which are otherwise no more than 2° apart. The third (right) panel of Fig. 13 compares the $N_{\max} = 17$ results for the previously discussed $V_{\text{low }k}$ and N^{3}LO NN interactions and those obtained with the CD-Bonn NN potential [39]. The NCSM/RGM calculations for the latter potential were carried out using two-body effective interactions and present a convergence pattern similar to the one observed for N^{3}LO. Clearly, the $^2P_{1/2}$ and $^2P_{3/2}$ phase shifts are sensitive to the interaction models and, in particular, to the strength of the spin-orbit force. This observation is in agreement with what was found in the earlier study of Ref. [9]. Following a behavior already observed in the structure of p-shell nuclei, CD-Bonn and N^{3}LO interactions yield about the same spin-orbit splitting. In contrast, the larger separation between the $V_{\text{low }k}$ $3/2^-$ and $1/2^-$ resonant phase shifts is direct evidence for a stronger spin-orbit interaction.

Because the $1/2^+$ channel is dominated by the repulsion between the neutron and the α particle induced by the Pauli exclusion principle (see also Sec. II D3), the short-range details of the nuclear interaction play a minor role on the $^2S_{1/2}$ phase shifts. As a consequence, we find very similar results for all of the three adopted NN potential models. Noteworthy is the different behavior of the CD-Bonn results close to zero energy, which appears also in the P waves.

Next we explore the effect of the inclusion of excited states of the ^{4}He on the n-α scattering phase shifts obtained with the N^{3}LO NN interaction. In contrast to the $A = 4$ scattering, discussed in the previous section, binary channels of the type $(A-2, 2)$ have here a much suppressed effect owing to the large binding energy of the ^{4}He nucleus. However, to reach full convergence it is still necessary to take into account the virtual excitations of the $A - 1 = 4$ target. To this aim we extend the NCSM/RGM SNP model space to include closed channels of the type $\nu = \{4\ 1\text{st ex.}\ I_1^{\pi_1}T_1;\ 1\ \frac{1}{2}^+\frac{1}{2};\ s\,\ell\}$ with $I_1^{\pi_1}T_1 = 0^+0$, 0^-0, 1^-1, 2^-0, and 2^-1, and "1st ex." specifies that, for each of these spin-parity and isospin combinations, we consider only the first (low-lying) excited state.

In addition to these single-channel results (dotted line), Figure 14 shows coupled-channel calculations for five different combinations of ^{4}He states: (i) g.s., 0^+0 (dash-dotted line), (ii) g.s., $0^+0, 0^-0$ (dash-dot-dotted line),

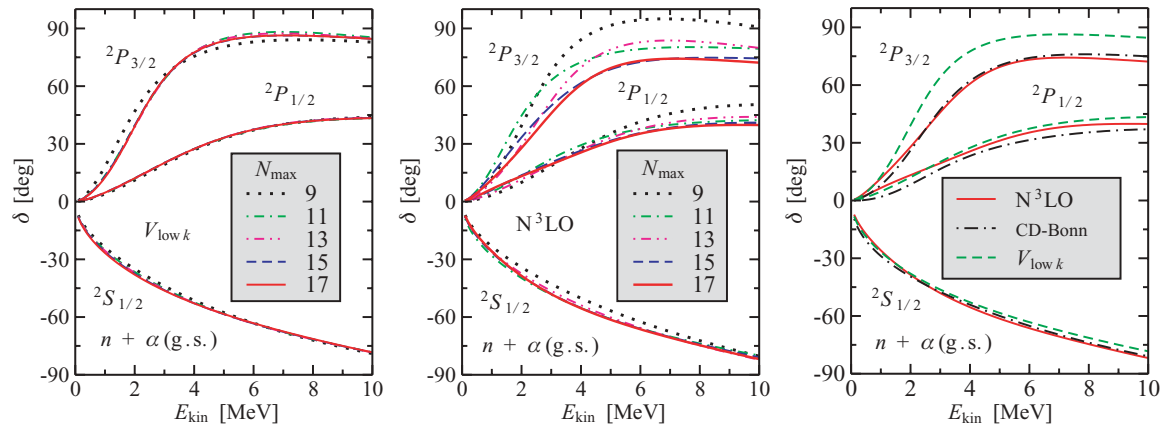

FIG. 13. (Color online) Dependence on $N_{\max}$ of the n-α(g.s.) phase shifts with the $V_{\text{low }k}$ [33] (left panel) and N^{3}LO [32] (central panel) NN potentials at $\hbar\Omega = 18$ and 19 MeV, respectively, along with the results obtained in the largest model space ($N_{\max} = 17$) (right panel). The calculation for the CD-Bonn [39] NN interaction was performed at $\hbar\Omega = 19$ MeV.

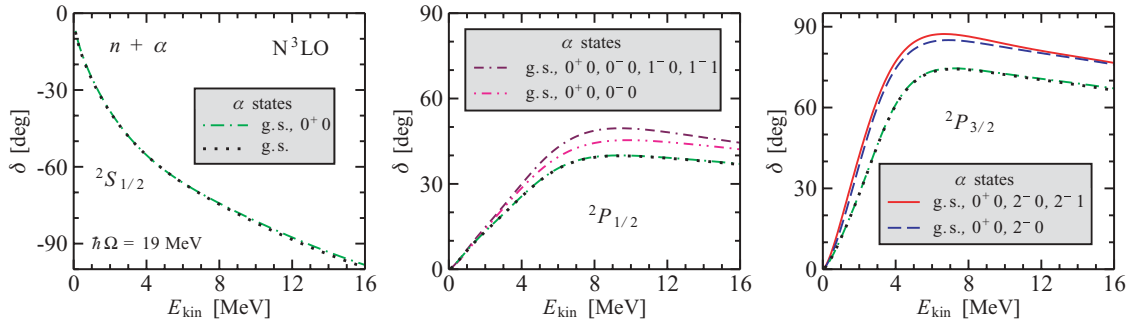

FIG. 14. (Color online) Influence of the lowest six excited states ($I_1^{\pi_1} T_1 = 0^+0, 0^-0, 1^-0, 1^-1, 2^-0, 2^-1$) of the α particle on the n-α $^2S_{1/2}$ (left panel), $^2P_{1/2}$ (central panel), and $^2P_{3/2}$ (right panel) phase-shift results for the N^{3}LO NN potential [32] at $\hbar\Omega = 19$ MeV. Dotted (g.s.) and dash-dotted (g.s., 0^+0) lines correspond to single- and coupled-channel calculations in an $N_{\max} = 17$ model space, respectively. The effects on the $^2P_{1/2}$ and $^2P_{3/2}$ phase shifts of the further inclusion of, respectively, the 0^-0, 1^-0, 1^-1, and 2^-0, 2^-1 states are investigated in an $N_{\max} = 15$ model space.

(iii) g.s., 0^+0, 0^-0, 1^-0, 1^-1 (dash-dash-dotted line), (iv) g.s., 0^+0, 2^-0 (dashed line), and (v) g.s., 0^+0, 2^-0, 2^-1 (solid line). The 0^+0 excited state has a minimal influence on all three phase shifts. In addition, for $^2S_{1/2}$ (left panel) no further corrections are found in the four larger Hilbert spaces obtained by including the low-lying negative-parity states of ^{4}He (but for clarity of the figure we omitted these latter $^2S_{1/2}$ results). In contrast, we find larger deviations on the $^2P_{1/2}$ (central panel) and $^2P_{3/2}$ (right panel) phase shifts, after inclusion of the 0^-0, 1^-0, and 1^-1 states for the first and of the 2^-0 and 2^-1 states for the second. These negative-parity states influence the P phase shifts, because they introduce couplings to the s wave of relative motion. Though also $I_1^{\pi_1} = 1^-$ couples to $\ell = 0$ in the $3/2^-$ channel, the coupling of the $I_1^{\pi_1} = 2^-$ states is dominant for the $^2P_{3/2}$ phase shifts.

Figure 15 provides further evidence that the NCSM/RGM SNP model space formed by nucleon-α binary channels with the α particle in its ground and first 0^+0 excited states is sufficient to reach full convergence of the $^2S_{1/2}$ phase shifts, also in presence of the Coulomb repulsion between proton and α particle. In the left panel, both n- and p-α N^{3}LO results show negligible dependence on the HO frequency, when varied from $\hbar\Omega = 19$ to 22 MeV. In the right panel, the latter phase shifts and the corresponding $V_{\text{low }k}$ and CD-Bonn $^2S_{1/2}$ results are compared to an accurate multichannel R-matrix analysis of nucleon-α scattering. The overall best agreement with experiment (which is quite remarkable for p-α) is obtained for the CD-Bonn NN interaction, where the different behavior of this potential near zero energy is favored by the data. The N^{3}LO phase shifts are not very dissimilar and reproduce the R-matrix analysis starting from an energy of roughly 2 MeV. The $V_{\text{low }k}$ interaction generates the largest deviation from experiment. Although these are "residual" reflections of the interaction details, otherwise masked by the Pauli exclusion principle, it becomes evident that scattering calculations can provide important additional constraints on the nuclear force.

A comparison to the R-matrix analysis of Ref. [40], including $^2P_{1/2}$, $^2P_{3/2}$, and $^2D_{3/2}$ partial waves, is presented in Fig. 16. Here, the n-α (left panel) and p-α (right panel) phase shifts were obtained with the N^{3}LO NN potential, including the first six ^{4}He excited states, as shown in Fig. 14. The magnitude of the $^2D_{3/2}$ phase shifts, calculated (as the $^2S_{1/2}$) in a NCSM/RGM SNP model space with ground and first 0^+0 excited states of the α particle, is qualitatively reproduced. In contrast, the P phase shifts present both insufficient magnitude and splitting with respect to the predictions of the R-matrix analysis. Although the inclusion of two more ^{4}He negative excited states (first 0^-1 and second 1^-1) beyond the five considered here could introduce small corrections, it is not likely that they would explain the present discrepancy with

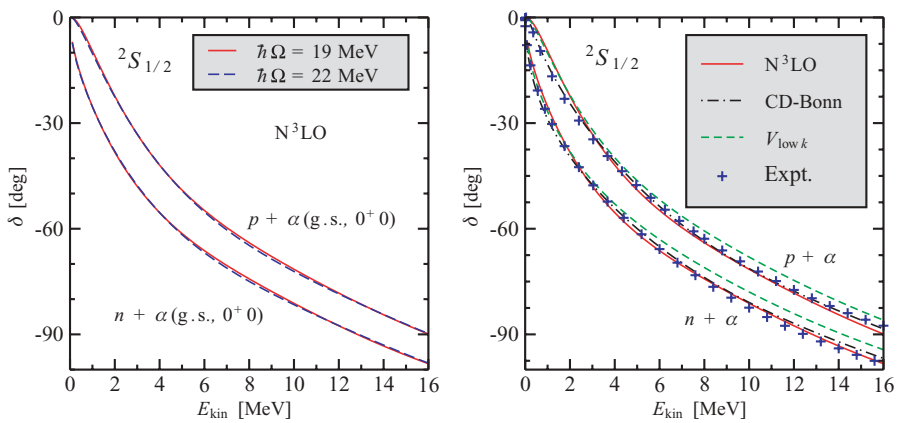

FIG. 15. (Color online) N-α $^2S_{1/2}$ phase shifts as a function of the relative kinetic energy in the c.m. frame, E_{kin}. The NCSM/RGM coupled-channel calculations include both ground and 0^+0 first excited states of the α particle, in a $N_{\max} = 17$ model space. Left and right panels show the frequency dependence, and a comparison to an R-matrix analysis of data (+) [40], respectively.

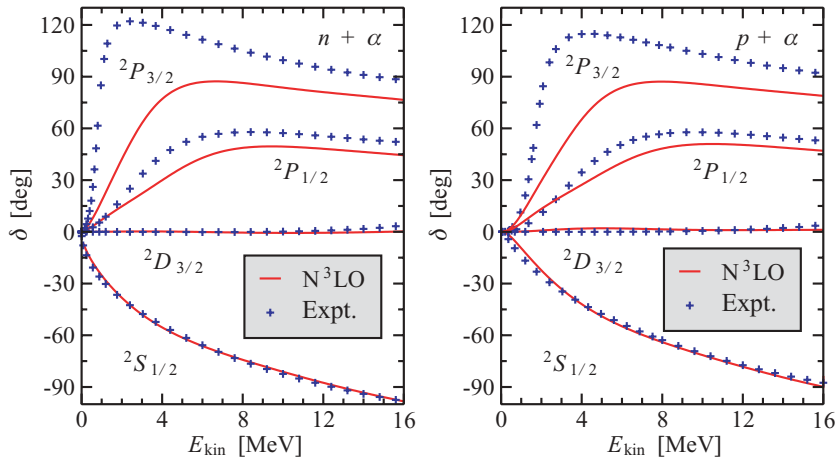

FIG. 16. (Color online) Calculated n-α (left panel) and p-α (right panel) phase shifts for the N^{3}LO NN potential [32] compared to an R-matrix analysis of data (+) [40]. $^2S_{1/2}$ results are as in Fig. 15. The $^2P_{1/2}$ and $^2P_{3/2}$ phase shifts correspond to the dash-dash-dotted (g.s., $0^+0, 0^-0, 1^-0, 1^-1$) and solid (g.s., $0^+0, 2^-0, 2^-1$) lines of Fig. 14. The $^2D_{3/2}$ phase shifts were obtained in a coupled-channel calculation including ground and first 0^+ excited states of ^{4}He, in an $N_{max} = 17$ HO model space.

respect to experiment of the $^2P_{1/2}$ and $^2P_{3/2}$ results. However, by considering the sensitivity of these phase shifts to the strength of the spin-orbit force, the inclusion of the NNN terms of the chiral interaction would probably lead to an enhanced spin-orbit splitting and recover the predictions of the R-matrix analysis.

C. $A = 11$

With the advent of experimental programs on exotic nuclei, the description of weakly bound nuclei has become one of the priorities of modern nuclear theory. As techniques traditionally successful for well-bound nuclei struggle to reproduce new phenomena observed in the radioactive-beam facilities, the interplay of structure and reaction mechanisms is now unanimously recognized as a prime element for a successful description of weakly bound nuclei. Such interplay is an intrinsic characteristic in the *ab initio* NCSM/RGM, where bound and scattering states are treated in a unified formalism. In this section we test the performance of our formalism in the SNP basis for the description of one-nucleon halo systems, and at the same time we show the versatility and promise of the NCSM/RGM for the description of the structure and reactions of p-shell nuclei.

Among light drip-line nuclei, ^{11}Be provides a convenient test of several important properties of neutron-rich nuclei. In particular, the parity-inverted ground state of this nucleus, first observed by Talmi and Unna in the early 1960s [41], represents one of the best examples of disappearance of the $N = 8$ magic number with increasing N/Z ratio.

The only previous *ab initio* investigations of the ^{11}Be low-lying states, consisting of large-scale NCSM calculations with realistic NN potentials, were unable to reproduce this phenomenon [42]. This result was partly attributed to the size of the HO basis, which was not large enough to reproduce the correct asymptotic of the n-^{10}Be component of the 11-body wave function. At the same time the calculations performed with the INOY (inside nonlocal outside Yukawa) NN potential of Doleschall and co-workers [43] suggested that the use of a realistic NNN force in a large NCSM basis might correct this discrepancy with experiment.

The correct asymptotic behavior of the n-^{10}Be wave functions can be reproduced when working within microscopic cluster techniques. Starting from a microscopic Hamiltonian containing the Volkov NN potential [44], the Coulomb interaction, and a zero-range spin-orbit force [45], Descouvemont was able to reproduce the inversion of the $1/2^+$ and $1/2^-$ ^{11}Be bound states within the generator coordinate method (GCM) [46]. However, the use of two different parametrizations of the Volkov potential for positive- and negative-parity states (chosen to reproduce, respectively, the experimental binding energies of the $1/2^+$ g.s. and $1/2^-$ first excited state) was key to this result. With a single parametrization for both parities, the lowest energy is obtained once again for the $1/2^-$ state, in contradiction with experiment. The introduction of the tensor force (missing in Ref. [46]) and the use of a richer structure for the ^{11}Be wave function could probably cure this problem.

A more complete bibliography on the ^{11}Be g.s. parity inversion and the theoretical attempts to reproduce it can be found in Refs. [42,46] and references therein.

Here, low-energy phase shifts for neutron scattering on ^{10}Be and low-lying levels of ^{11}Be are studied by means of NCSM/RGM coupled-channel calculations with n-^{10}Be channel states including the ^{10}Be ground and 2^+_1, 2^+_2, and 1^+_1 excited states (corresponding to channel indexes of the type $\nu = \{11\,\alpha_1\, I^{\pi_1}_1 T_1;\, 1\tfrac{1}{2}^+\tfrac{1}{2};\, s\,\ell\}$ with $\alpha_1\, I^{\pi_1}_1 T_1 =$ g.s. 0^+1, 1st ex. 2^+1, 2nd ex. 2^+1, and 1st ex. 1^+1). The NCSM ^{10}Be eigenstates, calculated for the first time in Ref. [47], are obtained here in a $N_{max} = 6$ model space. Correspondingly, the 11-body NCSM/RGM model space is $N_{max} = 6$ and 7 for negative- and positive-parity wave functions, respectively. To perform a direct comparison to the NCSM results for ^{11}Be [42] obtained using the CD-Bonn NN interaction [39], we adopt the same nuclear potential and optimal HO frequency, $\hbar\Omega = 13$ MeV.

In Table VI, we present energies of the lowest $1/2^+$ and $1/2^-$ states of ^{11}Be obtained in the NCSM and in the NCSM/RGM calculations. Clearly, there is little difference between the $N_{max} = 6/7$ and $N_{max} = 8/9$ NCSM results. The $1/2^-$ state is the ground state and the excitation energy of the $1/2^+$ state is about 3 MeV (or about 2.8 MeV above the n-^{10}Be threshold). The NCSM/RGM calculations that include

TABLE VI. Calculated energies (in MeV) of the ^{10}Be g.s. and of the lowest negative- and positive-parity states in ^{11}Be, obtained using the CD-Bonn NN potential [39] at $\hbar\Omega = 13$ MeV. The NCSM/RGM results were obtained using $n + {}^{10}$Be configurations with $N_{\max} = 6$ g.s., 2_1^+, 2_2^+, and 1_1^+ states of ^{10}Be.

	$N_{\max}$	^{10}Be	^{11}Be($\frac{1}{2}^-$)		^{11}Be($\frac{1}{2}^+$)	
		$E_{\text{g.s.}}$	E	E_{th}	E	E_{th}
NCSM [42,47]	8/9	−57.06	−56.95	0.11	−54.26	2.80
NCSM [42,47][a]	6/7	−57.17	−57.51	−0.34	−54.39	2.78
NCSM/RGM[a]			−57.59	−0.42	−57.85	−0.68
Expt.		−64.98	−65.16	−0.18	−65.48	−0.50

[a]Present calculation.

^{10}Be g.s. and the three lowest calculated excited states (2_1^+, 2_2^+, and 1_1^+) show little change for the energy of the $1/2^-$ state. However, we observe a dramatic decrease (∼3.5 MeV) of the energy of the $1/2^+$ state. In the NCSM/RGM calculations, both the $1/2^-$ and $1/2^+$ states are bound and the $1/2^+$ state becomes the ground state of ^{11}Be. To understand the binding mechanism of the $1/2^+$ state, we evaluated mean values of the relative kinetic and potential energies as well as the mean value of the ^{10}Be energy. The results are given in Table VII together with the corresponding values obtained by restricting all the kernels to the model space [i.e., by replacing the delta function of Eq. (35) with its representation in the HO model space]. The model-space-restricted calculation is then similar, although not identical, to the standard NCSM calculation. In particular, as in the NCSM one loses the correct asymptotic behavior of the wave functions, which is otherwise guaranteed in the NCSM/RGM. Because of the rescaling of the relative wave function in the internal region when the Whittaker tail is recovered, in the full NCSM/RGM calculation we observe that both relative kinetic and potential energies are smaller in absolute value. The drop is significantly more substantial for the relative kinetic energy than for the potential energy. This is the main cause of the dramatic decrease of the energy of the $1/2^+$ state, which makes it bound and even leads to a g.s. parity inversion. Although we cannot exclude that the NNN force plays a role in the inversion mechanism, it is clear that a proper treatment of the coupling to the n-^{10}Be continuum is essential in explaining the g.s. parity inversion.

Our calculated $^2S_{1/2}$ n-^{10}Be phase shifts are displayed in Fig. 17. We show results obtained with different number of ^{10}Be states. The phase shift does not change significantly, once the lowest 2^+ state is taken into account. A bound state was found, however, already by using just the ^{10}Be ground state. We also calculated the S-wave scattering length. With all four ^{10}Be states (g.s., 2_1^+, 2_2^+, and 1_1^+) included we found a $^2S_{1/2}$ scattering length of +10.7 fm. This can be compared to the value of +13.6 fm obtained in the GCM calculations of Ref. [46]. In those calculations, the ^{11}Be experimental binding energy of 0.5 MeV was fitted. Our calculated binding energy is slightly higher: 0.68 MeV. Correspondingly, our calculated scattering length is smaller.

In Fig. 18, we show our calculated $^2D_{5/2}$ n-^{10}Be phase shifts obtained using different number of ^{10}Be states. In this channel, we find a resonance below 3 MeV. To observe this resonance, it is crucial to include at least the first 2^+ excited state of ^{10}Be in the NCSM/RGM calculations. The restriction to just the ^{10}Be ground state results in a smooth slowly rising phase shift with no resonance at low energy. We note that a resonance has been experimentally observed at ∼1.8 MeV with a tentative spin assignment $(5/2, 3/2)^+$ [48].

The results presented in this section demonstrate the promise of the NCSM/RGM approach for applications to the p-shell nuclei. A significant improvement in the description of halo nuclei is achieved in particular when comparing to the standard NCSM calculations. The ^{11}Be and n-^{10}Be calculations discussed here were obtained in a limited model space. We will improve on this in the future by expanding the model-space sizes similarly as we did for the $A = 4$

TABLE VII. Mean values of the relative kinetic and potential energy and of the internal ^{10}Be energy in the ^{11}Be $1/2^+$ ground state. All energies in MeV. The NCSM/RGM calculation is as in Table VI. See the text for further details.

NCSM/RGM	$\langle T_{\text{rel}} \rangle$	$\langle W \rangle$	$E[^{10}\text{Be(g.s., ex.)}]$	E_{tot}
Model space	16.65	−15.02	−56.66	−55.03
Full	6.56	−7.39	−57.02	−57.85

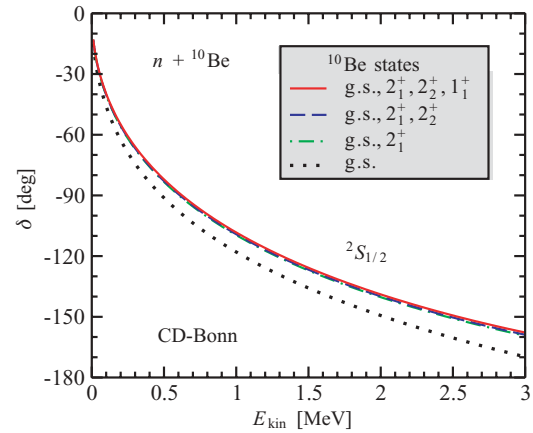

FIG. 17. (Color online) Calculated $^2S_{1/2}$ n-^{10}Be phase shifts as a function of E_{kin}, using the CD-Bonn NN potential. The NCSM/RGM calculation is as in Table VI. The obtained scattering length is +10.7 fm.

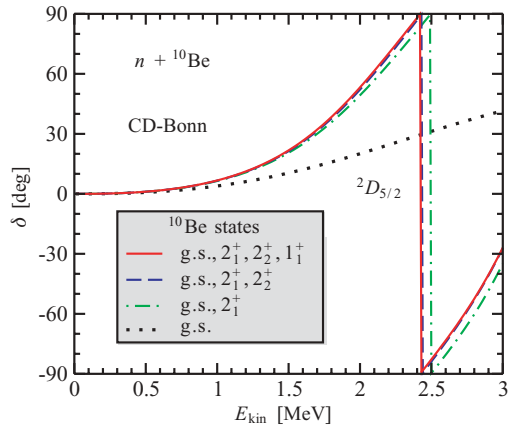

FIG. 18. (Color online) Calculated $^2D_{5/2}$ n-^{10}Be phase shifts as a function of $E_{\rm kin}$, using the CD-Bonn NN potential. The NCSM/RGM calculation is as in Table VI.

and $A = 5$ systems. This will also allow us to calculate reliably, for example, the P-wave scattering length predicted to have a very large value [49]. For light p-shell nuclei, it is presently feasible to perform calculations with $N_{\rm max} \sim 12$–16. For heavy and mid-p-shell nuclei, it becomes possible to employ the importance-truncated NCSM [50] to expand target wave functions in large $N_{\rm max}$ model spaces.

IV. CONCLUSIONS

We have presented in detail the NCSM/RGM formalism. This is a new *ab initio* many-body approach capable of describing simultaneously both bound and scattering states in light nuclei, by combining the RGM with the use of realistic interactions and a microscopic and consistent description of the nucleon clusters, achieved via the *ab initio* NCSM. In particular, we have derived the algebraic expressions for the integral kernels for the case of a single-nucleon projectile, working with both the Jacobi-coordinate and SD single-particle coordinate bases. As the spurious c.m. components present in the SD basis were removed exactly, in both frameworks the calculated integral kernels are translationally invariant and lead to identical results. Several analytical as well as numerical tests were performed to verify the approach, particularly by benchmarking independent Jacobi-coordinate and SD calculations for systems with up to five nucleons.

Among the applications, we presented results for neutron scattering on ^{3}H, ^{4}He, and ^{10}Be and proton scattering on ^{3,4}He, using realistic NN potentials. Our $A = 4$ scattering results were compared to earlier *ab initio* calculations. We found that the CD-Bonn NN potential in particular provides an excellent description of nucleon-^{4}He S-wave phase shifts. In contrast, the P-wave phase shifts that we obtained with any of the realistic NN potentials present both insufficient magnitude and splitting with respect to the R-matrix analysis of the data. It is anticipated that the inclusion of the NNN terms of the chiral interaction would lead to an enhanced spin-orbit splitting, and recover the predictions of the R-matrix analysis. An important topic of this work has been the investigation of the parity inversion of the ^{11}Be nucleus. Although we cannot exclude that, for example, the NNN force plays a role in the inversion mechanism, we have demonstrated that a proper treatment of the coupling to the n-^{10}Be continuum leads to a dramatic decrease of the energy of the $\frac{1}{2}^+$ state, which makes it bound and even leads to a g.s. parity inversion.

It is straightforward to extend the NCSM/RGM formalism to include two-nucleon (deuteron), three-nucleon (triton and ^{3}He), and four-nucleon (^{4}He) projectiles. Further, it is possible and desirable to extend the binary-cluster $(A - a, a)$ NCSM/RGM basis by the standard A-nucleon NCSM basis to unify the original *ab initio* NCSM and NCSM/RGM approaches. This will lead to a much faster convergence of the many-body calculations compared to the original approaches and, most importantly, to an optimal and balanced unified description of both bound and unbound states. Extensions of the approach to include three-body cluster channels are also among our future plans, and the feasibility of such a project is supported by recent developments on the treatment of both three-body bound and continuum states (see, e.g., Refs. [19–23]). In the NCSM/RGM a large HO basis expansion is needed not just for the convergence of the target and projectile eigenstates but also for the convergence of the localized parts of the integration kernels. The recently developed importance-truncated NCSM [50] makes it possible to use large $N_{\rm max}$ model spaces even for heavy p-shell nuclei and beyond. Using importance-truncated target wave functions within the NCSM/RGM formalism will allow us to reach for scattering calculations on heavier nuclei the same level of convergence obtained here for the $A = 4$ and $A = 5$ systems. The development of the two-to-four-nucleon projectile formalism, the unification of the NCSM/RGM with the standard NCSM, which we name *ab initio* NCSM with continuum (NCSMC), and applications of importance-truncated wave functions within the NCSM/RGM are underway.

ACKNOWLEDGMENTS

We thank A. Deltuva for providing AGS benchmark results, G. Hagen for providing $V_{{\rm low}\,k}$ matrix elements, J. Hale for supplying us with the nucleon-α phase shifts from the LANL R-matrix analysis, and S. Bacca, P. Descouvemont, and I. J. Thompson for valuable discussions. Numerical calculations have been performed at the LLNL LC facilities. Prepared by LLNL under Contract No. DE-AC52-07NA27344. Support from the US DOE/SC/NP (Work Proposal No. SCW0498), LLNL LDRD Grant No. PLS-09-ERD-020, and from the U. S. Department of Energy Grant No. DE-FC02-07ER41457 is acknowledged.

APPENDIX A: JACOBI-COORDINATE DERIVATION

1. $A = 3$

Continuing from Sec. II D1, where we have discussed the exchange part of the norm kernel, here we complete the

Jacobi-coordinate derivation of the integral kernels for the $A = 3$ ($a = 1$) system. For the notation we refer the interested reader to Eqs. (44)–(46).

As shown in Eq. (40), in the case of the "direct" potential kernel one needs to evaluate matrix elements of the interaction between the last two nucleons, $\langle V(\vec{r}_2 - \vec{r}_3, \sigma_2\sigma_3\tau_2\tau_3)(1 - \hat{P}_{23})\rangle$. It is therefore convenient to introduce two new Jacobi coordinates,

$$\vec{\zeta}_1 = \sqrt{\frac{2}{3}}\left[\frac{1}{2}(\vec{r}_2 + \vec{r}_3) - \vec{r}_1\right], \tag{A1}$$

$$\vec{\zeta}_2 = \frac{1}{\sqrt{2}}(\vec{r}_2 - \vec{r}_3), \tag{A2}$$

and switch to the HO basis states in which nucleons 2 and 3 are coupled together to form two-particle states of the form $\langle\zeta_2\sigma_2\sigma_3\tau_2\tau_3|N_2L_2S_2J_2T_2\rangle$, where N_2 and L_2 are the HO quantum numbers corresponding to the harmonic oscillator associated with $\vec{\zeta}_2$, and S_2, J_2, and T_2 are the two-nucleon spin, total angular momentum, and isospin quantum numbers of the (2,3)-nucleons couple, respectively. This task can be achieved, for example, by continuing from the expansion of Eq. (46):

$$\left\langle\vec{\xi}_1\vec{\eta}_2\sigma_1\sigma_2\sigma_3\middle|\left[(n_1\ell_1, n\ell)\Lambda; \left(s_1\tfrac{1}{2}\right)Z\right]J^\pi\right\rangle\left\langle\tau_1\tau_2\tau_3\middle|\left(T_1\tfrac{1}{2}\right)T\right\rangle$$

$$= \sum_{T_2}(-)^{\frac{3}{2}+T}\hat{T}_1\hat{T}_2\begin{Bmatrix}\frac{1}{2} & \frac{1}{2} & T_1\\ \frac{1}{2} & T & T_2\end{Bmatrix}\sum_{S_2}(-)^{\frac{3}{2}+Z}\hat{s}_1\hat{S}_2$$

$$\times\begin{Bmatrix}\frac{1}{2} & \frac{1}{2} & s_1\\ \frac{1}{2} & Z & S_2\end{Bmatrix}\sum_{N_2L_2,\mathcal{NL}}\langle N_2L_2, \mathcal{NL}, \Lambda|n\ell, n_1\ell_1, \Lambda\rangle_3$$

$$\times\sum_{\mathcal{J},J_2}\hat{L}\hat{Z}\hat{\mathcal{J}}\hat{J}_2\begin{Bmatrix}\mathcal{L} & \frac{1}{2} & \mathcal{J}\\ L_2 & S_2 & J_2\\ \Lambda & Z & J\end{Bmatrix}$$

$$\times\langle\vec{\zeta}_1\vec{\zeta}_2\sigma_1\sigma_2\sigma_3\tau_1\tau_2\tau_3|[\mathcal{NLJ}; N_2L_2S_2J_2T_2]J^\pi T\rangle. \tag{A3}$$

Here $\mathcal{N}, \mathcal{L}$, and $\mathcal{J}$ are the HO quantum numbers corresponding to the HO state associated with $\vec{\zeta}_1$ and the total angular momentum of the first nucleon with respect to the center of mass of the last two, respectively. Further, $\langle N_2L_2, \mathcal{NL}, \Lambda|n\ell, n_1\ell_1, \Lambda\rangle_3$ are the general HO brackets for two particles with mass ratio 3, which are the elements of the orthogonal transformation between the HO states $\langle\vec{\xi}_1\vec{\eta}_2|(n_1\ell_1, n\ell)\Lambda\rangle$ and $\langle\vec{\zeta}_1\vec{\zeta}_2|(\mathcal{NL}, N_2L_2)\Lambda\rangle$.

By combining the expansions of Eqs. (46) and (A3) it is possible to write the following expression for the $A = 3$ "direct" potential kernel in the SNP basis:

$$\mathcal{V}^{\mathrm{D}}_{\nu'\nu}(r', r)$$

$$= 2\sum_{n'n}R_{n'\ell'}(r', b)R_{n\ell}(r, b)\sum_{n'_1\ell'_1s'_1}\left\langle n'_1\ell'_1s'_1I'_1T'_1\middle|2\,\alpha'_1I'^{\pi'_1}_1T'_1\right\rangle$$

$$\times\sum_{n_1\ell_1s_1}\left\langle n_1\ell_1s_1I_1T_1\middle|2\,\alpha_1I^{\pi_1}_1T_1\right\rangle$$

$$\times(-)^{s'+s+I'_1+I_1+1}\hat{s}'_1\hat{s}_1\hat{I}'_1\hat{I}_1\hat{T}'_1\hat{T}_1\hat{s}'\hat{s}$$

$$\times\sum_{S_2J_2T_2}\hat{S}_2^2\hat{J}_2^2\hat{T}_2^2\begin{Bmatrix}\frac{1}{2} & \frac{1}{2} & T'_1\\ \frac{1}{2} & T & T_2\end{Bmatrix}\begin{Bmatrix}\frac{1}{2} & \frac{1}{2} & T_1\\ \frac{1}{2} & T & T_2\end{Bmatrix}$$

$$\times\sum_{\Lambda'\Lambda K}\hat{\Lambda}'^2\hat{\Lambda}^2\hat{K}^2(-)^{\Lambda'+\Lambda}\begin{Bmatrix}J & \frac{1}{2} & s'_1 & \ell'_1\\ K & \frac{1}{2} & I'_1 & \ell'\\ \Lambda' & S_2 & \frac{1}{2} & s'\end{Bmatrix}$$

$$\times\begin{Bmatrix}J & \frac{1}{2} & s_1 & \ell_1\\ K & \frac{1}{2} & I_1 & \ell\\ \Lambda & S_2 & \frac{1}{2} & s\end{Bmatrix}\sum_{N'_2L'_2}\sum_{N_2L_2}\sum_{\mathcal{NL}}\begin{Bmatrix}L'_2 & S_2 & J_2\\ K & \mathcal{L} & \Lambda'\end{Bmatrix}$$

$$\times\begin{Bmatrix}L_2 & S_2 & J_2\\ K & \mathcal{L} & \Lambda\end{Bmatrix}\langle N'_2L'_2, \mathcal{NL}, \Lambda'|n'\ell', n'_1\ell'_1, \Lambda'\rangle_3$$

$$\times\langle N_2L_2, \mathcal{NL}, \Lambda|n\ell, n_1\ell_1, \Lambda\rangle_3[1 - (-)^{L_2+S_2+T_2}]$$

$$\times\langle N'_2L'_2S_2J_2T_2|V(\sqrt{2}\vec{\zeta}_1\,\sigma_2\sigma_3\tau_2\tau_3)|N_2L_2S_2J_2T_2\rangle. \tag{A4}$$

Finally, for the $A = 3$ system, the "exchange" part of the potential kernel resembles closely the exchange part of the norm kernel and can be derived in a very similar way as the latter. Indeed, besides different multiplicative factors, Eqs. (37) and (41) differ only in the presence of the interaction between the second-to-last and next-to-last nucleons (the target nucleons in this case), the matrix elements of which can be easily calculated using the basis (44). Therefore, $A = 3$ "exchange" potential in the SNP basis is given by

$$\mathcal{V}^{\mathrm{ex}}_{\nu'\nu}(r', r)$$

$$= -2\sum_{n'n}R_{n'\ell'}(r')R_{n\ell}(r)\sum_{n'_1\ell'_1s'_1}\left\langle n'_1\ell'_1s'_1I'_1T'_1\middle|2\,\alpha'_1I'^{\pi'_1}_1T'_1\right\rangle$$

$$\times\sum_{n_1\ell_1s_1}\left\langle n_1\ell_1s_1I_1T_1\middle|2\,\alpha_1I^{\pi_1}_1T_1\right\rangle$$

$$\times\hat{T}'_1\hat{T}_1(-)^{T'_1+T_1}\begin{Bmatrix}\frac{1}{2} & \frac{1}{2} & T_1\\ \frac{1}{2} & T & T'_1\end{Bmatrix}\hat{s}'_1\hat{s}_1\hat{I}'_1\hat{I}_1\hat{s}'\hat{s}\,(-)^{\ell_1+\ell}$$

$$\times\sum_{\Lambda,Z}\hat{\Lambda}^2\hat{Z}^2(-)^{\Lambda}\begin{Bmatrix}\frac{1}{2} & \frac{1}{2} & s_1\\ \frac{1}{2} & Z & s'_1\end{Bmatrix}\begin{Bmatrix}\ell'_1 & Z & s'\\ J & \ell' & \Lambda\end{Bmatrix}$$

$$\times\begin{Bmatrix}\ell'_1 & Z & s'\\ \frac{1}{2} & I'_1 & s'_1\end{Bmatrix}\sum_{\mathcal{N}_1\mathcal{L}_1}\begin{Bmatrix}\mathcal{L}_1 & Z & s\\ J & \ell & \Lambda\end{Bmatrix}\begin{Bmatrix}\mathcal{L}_1 & Z & s\\ \frac{1}{2} & I_1 & s_1\end{Bmatrix}$$

$$\times\langle n'\ell', n'_1\ell'_1, \Lambda|\mathcal{N}_1\mathcal{L}_1, n\ell, \Lambda\rangle_3$$

$$\times\langle\mathcal{N}_1\mathcal{L}_1s_1I_1T_1|V(\sqrt{2}\xi_1\sigma_1\sigma_2\tau_1\tau_2)|n_1\ell_1s_1I_1T_1\rangle. \tag{A5}$$

Note that this expression can be easily reduced to the exchange part of the norm kernel by replacing $V(\sqrt{2}\xi_1\sigma_1\sigma_2\tau_1\tau_2)$ with 1.

2. $A \geqslant 4$

The expressions derived in this Appendix are valid for systems with $A \geqslant 4$ ($a = 1$).

We start by deriving the simplest of the integral kernels [i.e., the exchange part of the norm kernel (37)]. To this aim, it is convenient to expand the $(A-1)$-nucleon eigenstates $|A-1\,\alpha_1 I_1^{\pi_1} T_1\rangle$ onto a HO basis containing antisymmetric subclusters of $A-2$ nucleons, that is,

$$|(N_{A-2} i_{A-2} J_{A-2} T_{A-2}; n_{A-1}\ell_{A-1} j_{A-1}) I_1 T_1\rangle. \tag{A6}$$

Here, the antisymmetric states $|N_{A-2} i_{A-2} J_{A-2} T_{A-2}\rangle$ depend on the first $A-3$ Jacobi coordinates of Eq. (13) $(\vec{\xi}_1, \vec{\xi}_2, \ldots, \vec{\xi}_{A-3})$ and the first $A-2$ spin and isospin coordinates; they are characterized by the total number of HO excitations, spin, isospin, and additional quantum numbers $N_{A-2}, J_{A-2}, T_{A-2}$, and i_{A-2}, respectively. The basis states (A6) are not antisymmetrized with respect to the next-to-last nucleon, which is represented by the HO state $\langle \vec{\xi}_{A-2}\sigma_{A-1}\tau_{A-1}|n_{A-1}\ell_{A-1} j_{A-1}\rangle$, where n_{A-1}, ℓ_{A-1} are the HO quantum numbers corresponding to the harmonic oscillator associated with $\vec{\xi}_{A-2}$, and j_{A-1} is the angular momentum of the $(A-1)$th nucleon relative to the c.m. of the first $A-2$. In terms of the basis states (A6), the HO Jacobi channel state of Eq. (22) for the $(A-1, 1)$ system can be written as

$$\left|\Phi_{\nu n}^{J^\pi T}\right\rangle = \sum \left\langle (N_{A-2} i_{A-2} J_{A-2} T_{A-2}; n_{A-1}\ell_{A-1} j_{A-1}) I_1 T_1 \middle| A-1\,\alpha_1 I_1^{\pi_1} T_1 \right\rangle \times \left| \left[\left((N_{A-2} i_{A-2} J_{A-2} T_{A-2}; n_{A-1}\ell_{A-1} j_{A-1})\, I_1 T_1; \frac{1}{2}\frac{1}{2} \right) sT; n\ell \right] J^\pi T \right\rangle, \tag{A7}$$

where $\langle (N_{A-2} i_{A-2} J_{A-2} T_{A-2}; n_{A-1}\ell_{A-1} j_{A-1}) I_1 T_1 | A-1\,\alpha_1 I_1^{\pi_1} T_1\rangle$ are the coefficients of the expansion [25] of the $(A-1)$-cluster eigenstates on the basis (A6), and the sum runs over the quantum numbers $N_{A-2}, i_{A-2}, J_{A-2}, T_{A-2}, n_{A-1}, \ell_{A-1}$, and j_{A-1}.

According to Eq. (37), to obtain the exchange part of the norm kernel we need to evaluate matrix elements of the permutation corresponding to the exchange of the last two particles, $\hat{P}_{A-1,A}$. The task can be accomplished by, for example, switching to a more convenient coupling of the nucleon quantum numbers:

$$\left| \left[\left((N_{A-2} i_{A-2} J_{A-2} T_{A-2}; n_{A-1}\ell_{A-1} j_{A-1}) I_1 T_1; \frac{1}{2}\frac{1}{2} \right) sT; n\ell \right] J^\pi T \right\rangle = (-)^{J_{A-2}+I_1+\ell-\frac{1}{2}+2J} \hat{j}_{A-1}\hat{I}_1\hat{s} \sum_K \hat{K}(-)^K \sum_{\Lambda, S_2} \hat{\Lambda}\hat{S}_2 \begin{Bmatrix} \frac{1}{2} & S_2 & K & J_{A-2} \\ & \frac{1}{2} & \Lambda & J & I_1 \\ j_{A-1} & \ell_{A-1} & \ell & s & \end{Bmatrix} \times |[N_{A-2} i_{A-2} J_{A-2}; ((n_{A-1}\ell_{A-1}, n\ell)\Lambda\, S_2)K] J^\pi\rangle \left| \left(\left(T_{A-2}\frac{1}{2} \right) T_1 \frac{1}{2} \right) T \right\rangle, \tag{A8}$$

and observing that, as a result of the action of $\hat{P}_{A-1,A}$, the HO state $\langle \vec{\xi}_{A-2}\vec{\eta}_{A-1}|(n_{A-1}\ell_{A-1}, n\ell)\Lambda\rangle$ is changed into $\langle \vec{\xi}'_{A-2}\vec{\eta}'_{A-1}|(n_{A-1}\ell_{A-1}, n\ell)\Lambda\rangle$. (For a definition of the 12-j symbol see Appendix B.) The new set of Jacobi coordinates $\vec{\xi}'_{A-2}$ and $\vec{\eta}'_{A-1}$ (obtained from $\vec{\xi}_{A-2}$ and $\vec{\eta}_{A-1}$, respectively, by exchanging the single-nucleon indexes $A-1$ and A) can be expressed as an orthogonal transformation of the unprimed ones. Consequently, the HO states depending on them are related by the orthogonal transformation

$$\langle \vec{\xi}'_{A-2}\vec{\eta}'_{A-1}|(n_{A-1}\ell_{A-1}, n\ell)\Lambda\rangle = \sum_{NL, \mathcal{N}_{A-1}\mathcal{L}_{A-1}} \langle NL, \mathcal{N}_{A-1}\mathcal{L}_{A-1}, \Lambda | n_{A-1}\ell_{A-1}, n\ell, \Lambda\rangle_{A(A-2)} \times (-)^{L+\mathcal{L}_{A-1}-\Lambda} \langle \vec{\xi}_{A-2}\vec{\eta}_{A-1}|(\mathcal{N}_{A-1}\mathcal{L}_{A-1}, NL)\Lambda\rangle, \tag{A9}$$

where the elements of the transformation are the general HO brackets for two particles with mass ratio $d = A(A-2)$. After taking care of the action of $\hat{P}_{A-1,A}$ also on the spin and isospin coordinates, one can complete the derivation and write the following expression for the $A \geqslant 4$ exchange part of the norm kernel in the SNP basis:

$$\mathcal{N}_{\nu'\nu}^{\text{ex}}(r', r) = -(A-1) \sum_{n'n} R_{n'\ell'}(r') R_{n\ell}(r) \sum \left\langle (N_{A-2} i_{A-2} J_{A-2} T_{A-2}; n'_{A-1}\ell'_{A-1} j'_{A-1}) I'_1 T'_1 \middle| A-1\,\alpha'_1 I_1^{\prime\pi'_1} T'_1 \right\rangle$$

$$\times \left\langle (N_{A-2} i_{A-2} J_{A-2} T_{A-2}; n_{A-1} \ell_{A-1} j_{A-1}) I_1 T_1 \middle| A{-}1\, \alpha_1 I_1^{\pi_1} T_1 \right\rangle$$
$$\times \hat{T}_1' \hat{T}_1 (-)^{1+T_1'+T_1} \begin{Bmatrix} \frac{1}{2} & T_{A-2} & T_1 \\ \frac{1}{2} & T & T_1' \end{Bmatrix} \hat{j}'_{A-1} \hat{j}_{A-1} \hat{I}_1' \hat{I}_1 \hat{s}' \hat{s} (-)^{s'+s+\ell'_{A-1}+\ell} \sum_{\Lambda, Z} \hat{\Lambda}^2 \hat{Z}^2 (-)^{\Lambda} \begin{Bmatrix} j'_{A-1} & J_{A-2} & I_1' \\ j_{A-1} & Z & I_1 \end{Bmatrix}$$
$$\times \begin{Bmatrix} \ell'_{A-1} & \frac{1}{2} & j'_{A-1} \\ I_1 & Z & s \end{Bmatrix} \begin{Bmatrix} \ell_{A-1} & \frac{1}{2} & j_{A-1} \\ I_1' & Z & s' \end{Bmatrix} \begin{Bmatrix} \Lambda & \ell'_{A-1} & \ell' \\ \ell_{A-1} & Z & s' \\ \ell & s & J \end{Bmatrix} \langle n'\ell', n'_{A-1}\ell'_{A-1}, \Lambda | n_{A-1}\ell_{A-1}, n\ell, \Lambda \rangle_{A(A-2)}, \tag{A10}$$

where the second sum runs over the quantum numbers $N_{A-2}, i_{A-2}, J_{A-2}, T_{A-2}, n'_{A-1}, \ell'_{A-1}, j'_{A-1}, n_{A-1}, \ell_{A-1}$, and j_{A-1}. This expression was obtained by expanding the 12-j symbol of Eq. (A8) according to Eq. (B1) or (B1), and summing over the quantum numbers S_2 and K_2. Note that the norm kernel is symmetric under exchange of primed and unprimed indexes and coordinates.

We turn now to the derivation of the "direct" potential kernel of Eq. (40). As shown in Eq. (40), in this case one needs to evaluate matrix elements of the interaction between the last two nucleons, $\langle V(\vec{r}_{A-1} - \vec{r}_A, \sigma_{A-1}\sigma_A\tau_{A-1}\tau_A)(1 - \hat{P}_{A-1,A})\rangle$. It is therefore useful to introduce two new Jacobi coordinates,

$$\vec{\zeta}_{A-2} = \sqrt{\frac{2(A-2)}{A}} \left[\frac{1}{2}(\vec{r}_{A-1} + \vec{r}_A) - \frac{1}{A-2} \sum_{i=1}^{A-2} \vec{r}_i \right], \tag{A11}$$

$$\vec{\zeta}_{A-1} = \frac{1}{\sqrt{2}}(\vec{r}_{A-1} - \vec{r}_A), \tag{A12}$$

and switch to the HO basis states in which nucleons $A-1$ and A are coupled together to form two-particle states of the form $\langle \zeta_{A-1}\sigma_{A-1}\sigma_A\tau_{A-1}\tau_A | N_2 L_2 S_2 J_2 T_2 \rangle$, where N_2 and L_2 are the HO quantum numbers corresponding to the harmonic oscillator associated with $\vec{\zeta}_{A-1}$, and S_2, J_2, and T_2 are the two-nucleon spin, total angular momentum, and isospin quantum numbers of the $(A-1, A)$-nucleons couple, respectively. This task can be achieved, for example, by continuing from the expansion of Eq. (A8):

$$\langle \vec{\xi}_1 \cdots \vec{\xi}_{A-2} \vec{\eta}_{A-1} \sigma_1 \cdots \sigma_{A-1}\sigma_A | [N_{A-2} i_{A-2} J_{A-2}; ((n_{A-1}\ell_{A-1}, n\ell)\Lambda\, S_2) K] J^\pi \rangle \left\langle \tau_1 \cdots \tau_{A-1}\tau_A \middle| \left(\left(T_{A-2} \frac{1}{2} \right) T_1 \frac{1}{2} \right) T \right\rangle$$
$$= (-)^{1+T_{A-2}+T+S_2+K} \hat{T}_1 \hat{\Lambda} \sum_{T_2, J_2} \hat{T}_2 \hat{J}_2 \begin{Bmatrix} T_{A-2} & \frac{1}{2} & T_1 \\ \frac{1}{2} & T & T_2 \end{Bmatrix} \sum_{N_2 L_2, \mathcal{N}\mathcal{L}} (-)^{L_2+\mathcal{L}} \begin{Bmatrix} \mathcal{L} & L_2 & \Lambda \\ S_2 & K & J_2 \end{Bmatrix} \langle N_2 L_2, \mathcal{N}\mathcal{L}, \Lambda | n\ell, n_{A-1}\ell_{A-1}, \Lambda \rangle_{\frac{A}{A-2}}$$
$$\times \langle \vec{\xi}_1 \cdots \vec{\zeta}_{A-2} \vec{\zeta}_{A-1} \sigma_1 \cdots \sigma_{A-1}\sigma_A \tau_1 \cdots \tau_{A-1}\tau_A | [N_{A-2} i_{A-2} J_{A-2} T_{A-2}; (\mathcal{N}\mathcal{L}; N_2 L_2 S_2 J_2 T_2) K T_2] J^\pi T \rangle. \tag{A13}$$

At this point, the expression for the "direct" potential kernel can be easily derived by combining Eqs. (A6) and (A13), and observing that $V_{A-1,A}(1 - \hat{P}_{A-1,A})$ is diagonal in the quantum numbers $N_{A-2} i_{A-2} J_{A-2} T_{A-2}, \mathcal{N}\mathcal{L}$, and $S_2 J_2 T_2$:

$$\mathcal{V}^{\mathrm{D}}_{\nu'\nu}(r', r)$$
$$= (A-1) \sum_{n'n} R_{n'\ell'}(r') R_{n\ell}(r) \sum \left\langle (N_{A-2} i_{A-2} J_{A-2} T_{A-2}; n'_{A-1}\ell'_{A-1} j'_{A-1}) I_1' T_1' \middle| A{-}1\, \alpha_1' I_1'^{\pi_1'} T_1' \right\rangle$$
$$\times \left\langle (N_{A-2} i_{A-2} J_{A-2} T_{A-2}; n_{A-1}\ell_{A-1} j_{A-1}) I_1 T_1 \middle| A{-}1\, \alpha_1 I_1^{\pi_1} T_1 \right\rangle (-)^{1+2J+I_1'+I_1+\ell'+\ell} \hat{j}'_{A-1} \hat{j}_{A-1} \hat{I}_1' \hat{I}_1 \hat{T}_1' \hat{T}_1 \hat{s}' \hat{s}$$
$$\times \sum_{S_2, J_2, T_2} \hat{S}_2^2 \hat{J}_2^2 \hat{T}_2^2 \begin{Bmatrix} T_{A-2} & \frac{1}{2} & T_1' \\ \frac{1}{2} & T & T_2 \end{Bmatrix} \begin{Bmatrix} T_{A-2} & \frac{1}{2} & T_1 \\ \frac{1}{2} & T & T_2 \end{Bmatrix} \sum_K \hat{K}^2 \sum_{\Lambda', \Lambda} \hat{\Lambda}'^2 \hat{\Lambda}^2 \begin{Bmatrix} \frac{1}{2} & S_2 & K & J_{A-2} & \\ & \frac{1}{2} & \Lambda' & J & I_1' \\ j'_{A-1} & \ell'_{A-1} & \ell' & s' & \end{Bmatrix}$$

$$\times \left\{ \begin{array}{cccc} \frac{1}{2} & S_2 & K & J_{A-2} \\ \frac{1}{2} & \Lambda & J & I_1 \\ j_{A-1} & \ell_{A-1} & \ell & s \end{array} \right\} \sum_{\mathcal{NL}} \sum_{N_2' L_2' N_2 L_2} \langle N_2' L_2', \mathcal{NL}, \Lambda | n' \ell', n'_{A-1} \ell'_{A-1}, \Lambda' \rangle_{\frac{A}{A-2}} \langle N_2 L_2, \mathcal{NL}, \Lambda | n\ell, n_{A-1} \ell_{A-1}, \Lambda \rangle_{\frac{A}{A-2}}$$

$$\times \left\{ \begin{array}{ccc} \mathcal{L} & L_2' & \Lambda' \\ S_2 & K & J_2 \end{array} \right\} \left\{ \begin{array}{ccc} \mathcal{L} & L_2 & \Lambda \\ S_2 & K & J_2 \end{array} \right\} [1 - (-)^{L_2 + S_2 + T_2}] \langle N_2' L_2' S_2 J_2 T_2 | V(\sqrt{2} \vec{\zeta}_{A-1} \sigma_{A-1} \sigma_A \tau_{A-1} \tau_A) | N_2 L_2 S_2 J_2 T_2 \rangle, \tag{A14}$$

where the summation runs over the quantum numbers $N_{A-2}, i_{A-2}, J_{A-2}, T_{A-2}, n_{A-1}, \ell_{A-1}$, and j_{A-1}, as well as over the corresponding primed indexes.

Finally, we discuss the derivation of the "exchange" potential kernel [Eq. (41)]. The latter is a function of the matrix elements on the Jacobi channel states [Eq. (A7)] of the product of the $\hat{P}_{A-1,A}$ exchange operator and the interaction between the $(A-2)$th and $(A-1)$th nucleons: $\langle \Phi^{J^\pi T}_{\nu' n'} | \hat{P}_{A-1,A} \, V_{A-2,A-1} | \Phi^{J^\pi T}_{\nu n} \rangle$. Therefore one may proceed, for example, by first evaluating the action of $\hat{P}_{A-1,A}$ on the bra $\langle \Phi^{J^\pi T}_{\nu' n'} |$, and then the matrix elements of $V_{A-2,A-1}$ between the modified bra and the ket $|\Phi^{J^\pi T}_{\nu n}\rangle$. For the first step one can utilize (as done before for the "exchange" norm kernel), Eq. (A8). However, here, after the calculation of the action of the exchange operator, it is convenient to perform the inverse of the transformation of Eq. (A8) to return to the original coupling scheme of Eq. (A7). Indeed, the interaction $V_{A-2,A-1}$ acts on the $(A-1)$-cluster states and is diagonal in the quantum numbers n, ℓ, and s. The intermediate results resemble closely the expression of the exchange norm kernel and read

$$\begin{aligned}
&\mathcal{V}^{\rm ex}_{\nu' \nu}(r', r) \\
&= -(A-1)(A-2) \sum_{n' n} R_{n' \ell'}(r') R_{n \ell}(r) \sum \left\langle (N'_{A-2} i'_{A-2} J'_{A-2} T'_{A-2}; n'_{A-1} \ell'_{A-1} j'_{A-1}) I'_1 T'_1 \middle| A-1 \, \alpha'_1 I'^{\pi'_1}_1 T'_1 \right\rangle \\
&\quad \times \left\langle (N_{A-2} i_{A-2} J_{A-2} T_{A-2}; n_{A-1} \ell_{A-1} j_{A-1}) I_1 T_1 \middle| A-1 \, \alpha_1 I^{\pi_1}_1 T_1 \right\rangle \hat{T}'_1 \hat{T}_1 (-)^{1 + T'_1 + T_1} \left\{ \begin{array}{ccc} \frac{1}{2} & T'_{A-2} & T_1 \\ \frac{1}{2} & T & T'_1 \end{array} \right\} \\
&\quad \times \sum_{\mathcal{N}_{A-1} \mathcal{L}_{A-1} \mathcal{J}_{A-1}} \hat{j}'_{A-1} \hat{\mathcal{J}}_{A-1} \hat{I}'_1 \hat{I}_1 \hat{s}' \hat{s} (-)^{s' + s + \ell'_{A-1} + \ell} \sum_{\Lambda, Z} \hat{\Lambda}^2 \hat{Z}^2 (-)^{\Lambda} \left\{ \begin{array}{ccc} j'_{A-1} & J'_{A-2} & I'_1 \\ \mathcal{J}_{A-1} & Z & I_1 \end{array} \right\} \left\{ \begin{array}{ccc} \ell'_{A-1} & \frac{1}{2} & j'_{A-1} \\ I_1 & Z & s \end{array} \right\} \left\{ \begin{array}{ccc} \mathcal{L}_{A-1} & \frac{1}{2} & \mathcal{J}_{A-1} \\ I'_1 & Z & s' \end{array} \right\} \\
&\quad \times \left\{ \begin{array}{ccc} \Lambda & \ell'_{A-1} & \ell' \\ \mathcal{L}_{A-1} & Z & s' \\ \ell & s & J \end{array} \right\} \langle n\ell, \mathcal{N}_{A-1} \mathcal{L}_{A-1}, \Lambda | n'_{A-1} \ell'_{A-1}, n' \ell', \Lambda \rangle_{A(A-2)} \\
&\quad \times \left\langle (N'_{A-2} i'_{A-2} J'_{A-2} T'_{A-2}; \mathcal{N}_{A-1} \mathcal{L}_{A-1} \mathcal{J}_{A-1}) I_1 T_1 \middle| V_{A-2,A-1} \middle| (N_{A-2} i_{A-2} J_{A-2} T_{A-2}; n_{A-1} \ell_{A-1} j_{A-1}) I_1 T_1 \right\rangle,
\end{aligned} \tag{A15}$$

where the summation runs over both the primed and unprimed sets of quantum numbers $N'_{A-2}, i'_{A-2}, J'_{A-2}, T'_{A-2}$, $n'_{A-1}, \ell'_{A-1}, j'_{A-1}$ and $N_{A-2}, i_{A-2}, J_{A-2}, T_{A-2}, n_{A-1}, \ell_{A-1}$, j_{A-1}. Note that, by replacing $V_{A-2,A-1}$ with 1, one correctly recovers the exchange part of the norm kernel [Eq. (A10)]. For the second step, that is, the evaluation of the matrix elements of the interaction between the second- and next-to-last nucleons, $V(\vec{r}_{A-2} - \vec{r}_{A-1}, \sigma_{A-2} \sigma_{A-1} \tau_{A-2} \tau_{A-1})$, we introduce two new Jacobi coordinates, namely

$$\vec{\rho}_{A-3} = \sqrt{\frac{2(A-3)}{A-1}} \left[\frac{1}{A-3} \sum_{i=1}^{A-3} \vec{r}_i - \frac{1}{2} (\vec{r}_{A-2} + \vec{r}_{A-1}) \right] \tag{A16}$$

and

$$\vec{\rho}_{A-2} = \frac{1}{\sqrt{2}} (\vec{r}_{A-2} - \vec{r}_{A-1}), \tag{A17}$$

and switch to the HO basis states in which nucleons $A-2$ and $A-1$ are coupled together to form two-particle states of the form $\langle \vec{\rho}_{A-2} \sigma_{A-2} \sigma_{A-1} \tau_{A-2} \tau_{A-1} | n_2 \ell_2 s_2 j_2 t_2 \rangle$, where n_2 and ℓ_2 are the HO quantum numbers corresponding to the harmonic oscillator associated with $\vec{\rho}_{A-2}$, and s_2, j_2, and t_2 are the two-nucleon spin, total angular momentum, and isospin quantum

numbers, respectively:

$$
\begin{aligned}
&\langle \vec{\xi}_1 \cdots \vec{\xi}_{A-3}\vec{\xi}_{A-2}\sigma_1 \cdots \sigma_{A-3}\sigma_{A-2}\tau_1 \cdots \tau_{A-3}\tau_{A-2}|(N_{A-2}i_{A-2}J_{A-2}T_{A-2}; n_{A-1}\ell_{A-1}j_{A-1})I_1T_1\rangle \\
&\quad = \sum \langle N_{A-3}i_{A-3}J_{A-3}T_{A-3}; n_{A-2}\ell_{A-2}j_{A-2}||N_{A-2}i_{A-2}J_{A-2}T_{A-2}\rangle (-)^{T_{A-3}+T_1}\,\hat{T}_{A-2}(-)^{j_{A-2}+j_{A-1}+J_{A-3}+I_1}\,\hat{J}_{A-2}\hat{j}_{A-2}\hat{j}_{A-1} \\
&\qquad \times \sum_Y \hat{Y} \begin{Bmatrix} J_{A-3} & j_{A-2} & J_{A-2} \\ j_{A-1} & I_1 & Y \end{Bmatrix} \sum_{s_2 j_2 t_2} \hat{s}_2 \hat{j}_2 \hat{t}_2 (-)^{j_2+t_2} \begin{Bmatrix} T_{A-3} & \frac{1}{2} & T_{A-2} \\ \frac{1}{2} & T_1 & t_2 \end{Bmatrix} \sum_\lambda \hat{\lambda}^2 \begin{Bmatrix} \ell_{A-2} & \frac{1}{2} & j_{A-2} \\ \ell_{A-1} & \frac{1}{2} & j_{A-1} \\ \lambda & s_2 & Y \end{Bmatrix} \sum_{n_1\ell_1, n_2\ell_2} \begin{Bmatrix} \ell_1 & \ell_2 & \lambda \\ s_2 & Y & j_2 \end{Bmatrix} \\
&\qquad \times \langle n_2\ell_2, n_1\ell_1, \lambda | n_{A-1}\ell_{A-1}, n_{A-2}\ell_{A-2}, \lambda\rangle_{\frac{A-1}{A-3}} \\
&\qquad \times \langle \vec{\xi}_1 \cdots \vec{\rho}_{A-3}\vec{\rho}_{A-2}\sigma_1 \cdots \sigma_{A-2}\sigma_{A-1}\tau_1 \cdots \tau_{A-2}\tau_{A-1}|(N_{A-3}i_{A-3}J_{A-3}T_{A-3}; (n_1\ell_1; n_2\ell_2 s_2 j_2 t_2)Y t_2)I_1T_1\rangle. \qquad \text{(A18)}
\end{aligned}
$$

In deriving this expression, we have expanded the $(A-2)$-nucleon antisymmetric states $|N_{A-2}i_{A-2}J_{A-2}T_{A-2}\rangle$ onto a basis containing an antisymmetric subcluster of $A-3$ nucleons, using the coefficient of fractional parentage $\langle N_{A-3}i_{A-3}J_{A-3}T_{A-3};\, n_{A-2}\ell_{A-2}j_{A-2}||N_{A-2}i_{A-2}J_{A-2}T_{A-2}\rangle$. The summation is intended over the quantum numbers N_{A-3}, i_{A-3}, J_{A-3}, T_{A-3}, n_{A-2}, ℓ_{A-2}, and j_{A-2}.

In this basis,which is not antisymmetric for exchanges of the $(A-2)$th nucleon, the antisymmetric $|N_{A-3}i_{A-3}J_{A-3}T_{A-3}\rangle$ states depend on the first $A-4$ Jacobi coordinates of Eq. (13) $(\vec{\xi}_1, \vec{\xi}_2, \cdots, \vec{\xi}_{A-4})$ and the first $A-3$ spin and isospin coordinates. Here N_{A-3}, J_{A-3}, T_{A-3}, and i_{A-3} are the total number of HO excitations, spin, isospin, and additional quantum number characterizing the $(A-3)$-nucleon antisymmetric basis states, respectively. The second-to-last nucleon is represented by the HO state $\langle \vec{\xi}_{A-3}\sigma_{A-2}\tau_{A-2}|n_{A-2}\ell_{A-2}j_{A-2}\rangle$, where n_{A-2} and ℓ_{A-2} are the HO quantum numbers corresponding to the harmonic oscillator associated with $\vec{\xi}_{A-3}$, and j_{A-2} is the angular momentum of the $(A-2)$th nucleon relative to the c.m. of the first $A-3$ nucleons. The summation in Eq. (A18) runs over the quantum numbers N_{A-3}, J_{A-3}, T_{A-3}, i_{A-3}, n_{A-2}, ℓ_{A-2}, and j_{A-2}. Further, $\langle n_2\ell_2, n_1\ell_1, \lambda|n_{A-2}\ell_{A-2}, n_{A-1}\ell_{A-1}, \lambda\rangle_{(A-1)/(A-3)}$ are the general HO brackets for two particles with mass ratio $d = (A-1)/(A-3)$, which are the elements of the orthogonal transformation between the HO states $\langle \vec{\xi}_{A-3}\vec{\xi}_{A-2}|(n_{A-2}\ell_{A-2}, n_{A-1}\ell_{A-1})\lambda\rangle$ and $\langle \vec{\rho}_{A-3}\vec{\rho}_{A-2}|(n_1\ell_1, n_2\ell_2)\lambda\rangle$.

It is now trivial to complete the derivation of the "exchange" potential kernel by complementing Eq. (A15) with the following expression:

$$
\begin{aligned}
&\left\langle (N'_{A-2}i'_{A-2}J'_{A-2}T'_{A-2}; \mathcal{N}_{A-1}\mathcal{L}_{A-1}\mathcal{J}_{A-1})I_1T_1 \middle| V_{A-2,A-1} \middle| (N_{A-2}i_{A-2}J_{A-2}T_{A-2}; n_{A-1}\ell_{A-1}j_{A-1})I_1T_1 \right\rangle \\
&\quad = \sum \langle N_{A-3}i_{A-3}J_{A-3}T_{A-3}; n'_{A-2}\ell'_{A-2}j'_{A-2}||N'_{A-2}i'_{A-2}J'_{A-2}T'_{A-2}\rangle \langle N_{A-3}i_{A-3}J_{A-3}T_{A-3}; n_{A-2}\ell_{A-2}j_{A-2}||N_{A-2}i_{A-2}J_{A-2}T_{A-2}\rangle \\
&\qquad \times (-)^{j'_{A-2}+j_{A-2}+\mathcal{J}_{A-1}+j_{A-1}} \hat{j}'_{A-2}\hat{j}_{A-2}\hat{\mathcal{J}}_{A-1}\hat{j}_{A-1}\hat{J}'_{A-2}\hat{J}_{A-2}\hat{T}'_{A-2}\hat{T}_{A-2} \sum_{s_2 j_2 t_2} \hat{s}_2^2 \hat{j}_2^2 \hat{t}_2^2 \begin{Bmatrix} T_{A-3} & \frac{1}{2} & T'_{A-2} \\ \frac{1}{2} & T_1 & t_2 \end{Bmatrix} \begin{Bmatrix} T_{A-3} & \frac{1}{2} & T_{A-2} \\ \frac{1}{2} & T_1 & t_2 \end{Bmatrix} \\
&\qquad \times \sum_Y \hat{Y}^2 \sum_{\lambda',\lambda} \hat{\lambda}'^2 \hat{\lambda}^2 \begin{Bmatrix} J_{A-3} & j'_{A-2} & J'_{A-2} \\ \mathcal{J}_{A-1} & I_1 & Y \end{Bmatrix} \begin{Bmatrix} J_{A-3} & j_{A-2} & J_{A-2} \\ j_{A-1} & I_1 & Y \end{Bmatrix} \begin{Bmatrix} \ell'_{A-2} & \frac{1}{2} & j'_{A-2} \\ \mathcal{L}_{A-1} & \frac{1}{2} & \mathcal{J}_{A-1} \\ \lambda' & s_2 & Y \end{Bmatrix} \begin{Bmatrix} \ell_{A-2} & \frac{1}{2} & j_{A-2} \\ \ell_{A-1} & \frac{1}{2} & j_{A-1} \\ \lambda & s_2 & Y \end{Bmatrix} \\
&\qquad \times \sum_{n_1\ell_1} \sum_{n'_2\ell'_2} \sum_{n_2\ell_2} \langle n'_2\ell'_2, n_1\ell_1, \lambda'|\mathcal{N}_{A-1}\mathcal{L}_{A-1}, n'_{A-2}\ell'_{A-2}, \lambda'\rangle_{\frac{A-1}{A-3}} \langle n_2\ell_2, n_1\ell_1, \lambda|n_{A-1}\ell_{A-1}, n_{A-2}\ell_{A-2}, \lambda\rangle_{\frac{A-1}{A-3}} \\
&\qquad \times \begin{Bmatrix} \ell_1 & \ell'_2 & \lambda' \\ s_2 & Y & j_2 \end{Bmatrix} \begin{Bmatrix} \ell_1 & \ell_2 & \lambda \\ s_2 & Y & j_2 \end{Bmatrix} \langle n'_2\ell'_2 s_2 j_2 t_2|V(\sqrt{2}\vec{\rho}_{A-2}\sigma_{A-2}\sigma_{A-1}\tau_{A-2}\tau_{A-1})|n_2\ell_2 s_2 j_2 t_2\rangle, \qquad \text{(A19)}
\end{aligned}
$$

where the summation runs over he quantum numbers $N_{A-3}, i_{A-3}, J_{A-3}, T_{A-3}, n_{A-2}, \ell_{A-2}, j_{A-2}, n'_{A-2}, \ell'_{A-2}$, and j'_{A-2}.

For $A = 4$ $(a = 1)$ the $(A-2)$-nucleon states $|N_{A-2} i_{A-2} J_{A-2} T_{A-2}\rangle$ are simply antisymmetric two-nucleon states of the kind $|N_2 L_2 S_2 J_2 T_2\rangle$ characterized by a single Jacobi coordinate $(\vec{\xi}_1)$. Therefore, the transformation (A18) is somewhat different for the four-nucleon system, leading to an independent expression for the matrix elements of the $V_{2,3}$ interaction term between the target basis states:

$$
\begin{aligned}
&\langle (N'_2 L'_2 S'_2 J'_2 T'_2; \mathcal{N}_3 \mathcal{L}_3 \mathcal{J}_3) I_1 T_1 | V_{2,3} | N_2 L_2 S_2 J_2 T_2; n_3 \ell_3 j_3) I_1 T_1 \rangle \\
&= \frac{1}{2}\left[1 - (-1)^{L'_2 + S'_2 + T'_2}\right] \frac{1}{2}\left[1 - (-1)^{L_2 + S_2 + T_2}\right] (-1)^{S'_2 + S_2} \hat{J}'_2 \hat{J}_2 \hat{\mathcal{J}}_3 \hat{j}_3 \hat{T}'_2 \hat{T}_2 \sum_{s_2 j_2 t_2} \hat{s}_2^2 \hat{j}_2^2 \hat{t}_2^2 \begin{Bmatrix} \frac{1}{2} & \frac{1}{2} & T'_2 \\ \frac{1}{2} & T_1 & t_2 \end{Bmatrix} \begin{Bmatrix} \frac{1}{2} & \frac{1}{2} & T_2 \\ \frac{1}{2} & T_1 & t_2 \end{Bmatrix} \\
&\times \sum_Y \hat{Y}^2 \sum_{\lambda', \lambda} \hat{\lambda}'^2 \hat{\lambda}^2 \begin{Bmatrix} \frac{1}{2} & \mathcal{J}_3 & I_1 & Y \\ \mathcal{L}_3 & J'_2 & \frac{1}{2} & s_2 \\ \lambda' & L'_2 & S'_2 & \frac{1}{2} \end{Bmatrix} \begin{Bmatrix} \frac{1}{2} & j_3 & I_1 & Y \\ \ell_3 & J_2 & \frac{1}{2} & s_2 \\ \lambda & L_2 & S_2 & \frac{1}{2} \end{Bmatrix} \\
&\times \sum_{n_1 \ell_1} \sum_{n'_2 \ell'_2} \sum_{n_2 \ell_2} \langle n'_2 \ell'_2, n_1 \ell_1, \lambda' | \mathcal{N}_3 \mathcal{L}_3, N'_2 L'_2, \lambda' \rangle_3 \langle n_2 \ell_2, n_1 \ell_1, \lambda | n_3 \ell_3, N_2 L_2, \lambda \rangle_3 \begin{Bmatrix} \ell_1 & \ell'_2 & \lambda' \\ s_2 & Y & j_2 \end{Bmatrix} \\
&\times \begin{Bmatrix} \ell_1 & \ell_2 & \lambda \\ s_2 & Y & j_2 \end{Bmatrix} \langle n'_2 \ell'_2 s_2 j_2 t_2 | V(\sqrt{2}\vec{\rho}_2 \sigma_2 \sigma_3 \tau_2 \tau_3) | n_2 \ell_2 s_2 j_2 t_2 \rangle . \qquad \text{(A20)}
\end{aligned}
$$

Note that to recover the full expression for the $A = 4\,(a = 1)$ "exchange" potential kernel, it is sufficient to replace A with 4 in Eq. (A15) and combine the latter equation with Eq. (A20).

APPENDIX B: 12-j SYMBOL DEFINITION

The 12-j symbol of the first kind [51] is defined by

$$
\begin{Bmatrix} e & h & b & c \\ r & s & p & q \\ s & g & a & d \end{Bmatrix}
$$

$$
\begin{aligned}
&= \sum_X (-1)^{a+b+c+d+e+f+g+h+p+q+r+s-X} \hat{X}^2 \begin{Bmatrix} a & b & X \\ c & d & p \end{Bmatrix} \\
&\times \begin{Bmatrix} c & d & X \\ e & f & q \end{Bmatrix} \begin{Bmatrix} e & f & X \\ g & h & r \end{Bmatrix} \begin{Bmatrix} g & h & X \\ b & a & s \end{Bmatrix} \qquad \text{(B1)} \\
&= \sum_Y (-1)^{2Y+a+b+e+f} \hat{Y}^2 \begin{Bmatrix} s & h & b \\ g & r & f \\ a & e & Y \end{Bmatrix} \begin{Bmatrix} b & f & Y \\ q & p & c \end{Bmatrix} \begin{Bmatrix} a & e & Y \\ q & p & d \end{Bmatrix} . \qquad \text{(B2)}
\end{aligned}
$$

[1] H. Kamada *et al.*, Phys. Rev. C **64**, 044001 (2001).
[2] A. Nogga, H. Kamada, and W. Glöckle, Phys. Rev. Lett. **85**, 944 (2000).
[3] R. B. Wiringa, S. C. Pieper, J. Carlson, and V. R. Pandharipande, Phys. Rev. C **62**, 014001 (2000); S. C. Pieper and R. B. Wiringa, Annu. Rev. Nucl. Part. Sci. **51**, 53 (2001); S. C. Pieper, K. Varga, and R. B. Wiringa, Phys. Rev. C **66**, 044310 (2002).
[4] P. Navrátil and W. E. Ormand, Phys. Rev. C **68**, 034305 (2003).
[5] H. Witala, W. Glöckle, J. Golak, A. Nogga, H. Kamada, R. Skibinski, and J. Kuros-Zolnierczuk, Phys. Rev. C **63**, 024007 (2001).
[6] R. Lazauskas and J. Carbonell, Phys. Rev. C **70**, 044002 (2004).
[7] A. Kievsky, S. Rosati, M. Viviani, L. E. Marcucci, and L. Girlanda, J. Phys. G **35**, 063101 (2008).
[8] A. Deltuva and A. C. Fonseca, Phys. Rev. C **75**, 014005 (2007); Phys. Rev. Lett. **98**, 162502 (2007).
[9] K. M. Nollett, S. C. Pieper, R. B. Wiringa, J. Carlson, and G. M. Hale, Phys. Rev. Lett. **99**, 022502 (2007).
[10] K. Wildermuth and Y. C. Tang, *A Unified Theory of the Nucleus* (Vieweg, Braunschweig, 1977).
[11] Y. C. Tang, M. LeMere, and D. R. Thompson, Phys. Rep. **47**, 167 (1978).
[12] T. Fliessbach and H. Walliser, Nucl. Phys. **A377**, 84 (1982).
[13] K. Langanke and H. Friedrich, in *Advances in Nuclear Physics*, edited by J. W. Negele and E. Vogt (Plenum, New York, 1986), p. 223.
[14] R. G. Lovas, R. J. Liotta, A. Insolia, K. Varga, and D. S. Delion, Phys. Rep. **294**, 265 (1998).
[15] H. M. Hofmann and G. M. Hale, Phys. Rev. C **77**, 044002 (2008).
[16] P. Navrátil, J. P. Vary, and B. R. Barrett, Phys. Rev. Lett. **84**, 5728 (2000); Phys. Rev. C **62**, 054311 (2000).
[17] S. Quaglioni and P. Navrátil, Phys. Rev. Lett. **101**, 092501 (2008).
[18] P. Navrátil, C. A. Bertulani, and E. Caurier, Phys. Lett. **B634**, 191 (2006); Phys. Rev. C **73**, 065801 (2006); Nucl. Phys. **A787**, 539c (2007).
[19] P. Descouvemont, C. Daniel, and D. Baye, Phys. Rev. C **67**, 044309 (2003).

[20] P. Descouvemont, E. Tursunov, and D. Baye, Nucl. Phys. **A765**, 370 (2006).
[21] M. Theeten, D. Baye, and P. Descouvemont, Phys. Rev. C **74**, 044304 (2006).
[22] M. Theeten, H. Matsumura, M. Orabi, D. Baye, P. Descouvemont, Y. Fujiwara, and Y. Suzuki, Phys. Rev. C **76**, 054003 (2007).
[23] D. Baye, P. Capel, P. Descouvemont, and Y. Suzuki, Phys. Rev. C **79**, 024607 (2009).
[24] P. Navrátil and B. R. Barrett, Phys. Rev. C **57**, 562 (1998).
[25] P. Navrátil, G. P. Kamuntavičius, and B. R. Barrett, Phys. Rev. C **61**, 044001 (2000).
[26] P. Navrátil, Phys. Rev. C **70**, 014317 (2004).
[27] P. Navrátil, Phys. Rev. C **70**, 054324 (2004).
[28] K. Suzuki and S. Y. Lee, Prog. Theor. Phys. **64**, 2091 (1980).
[29] E. Caurier, G. Martinez-Pinedo, F. Nowacki, A. Poves, J. Retamosa, and A. P. Zuker, Phys. Rev. C **59**, 2033 (1999); E. Caurier and F. Nowacki, Acta Phys. Pol. B **30**, 705 (1999).
[30] J. P. Vary, The Many-Fermion-Dynamics Shell-Model Code, Iowa State University, 1992 (unpublished).
[31] L. Trlifaj, Phys. Rev. C **5**, 1534 (1972).
[32] D. R. Entem and R. Machleidt, Phys. Rev. C **68**, 041001(R) (2003).
[33] S. K. Bogner, T. T. S. Kuo, and A. Schwenk, Phys. Rep. **386**, 1 (2003); G. Hagen (private communication).
[34] S. Quaglioni and P. Navrátil, Phys. Lett. **B652**, 370 (2007).
[35] H. Kamada, S. Oryu, and A. Nogga, Phys. Rev. C **62**, 034004 (2000).
[36] M. Hesse, J.-M. Sparenberg, F. Van Raemdonck, and D. Baye, Nucl. Phys. **A640**, 37 (1998); M. Hesse, J. Roland, and D. Baye, *ibid.* **A709**, 184 (2002).
[37] A. Deltuva, A. C. Fonseca, and P. U. Sauer, Phys. Rev. C **71**, 054005 (2005); **72**, 054004 (2005); Phys. Rev. Lett. **95**, 092301 (2005).
[38] A. Deltuva (private communication).
[39] R. Machleidt, Phys. Rev. C **63**, 024001 (2001).
[40] G. M. Hale (private communication).
[41] I. Talmi and I. Unna, Phys. Rev. Lett. **4**, 469 (1960).
[42] C. Forssén, P. Navrátil, W. E. Ormand, and E. Caurier, Phys. Rev. C **71**, 044312 (2005).
[43] P. Doleschall, Phys. Rev. C **69**, 054001 (2004); P. Doleschall, I. Borbély, Z. Papp, and W. Plessas, *ibid.* **67**, 064005 (2003).
[44] A. B. Volkov, Nucl. Phys. **74**, 33 (1965).
[45] D. Baye and N. Pecher, Bull. Cl. Sci. Acad. Roy. Belg. **67**, 835 (1981).
[46] P. Descouvemont, Nucl. Phys. **A615**, 261 (1997).
[47] E. Caurier, P. Navrátil, W. E. Ormand, and J. P. Vary, Phys. Rev. C **66**, 024314 (2002).
[48] F. Ajzenberg-Selove, Nucl. Phys. **A506**, 1 (1990).
[49] S. Typel and G. Baur, Phys. Rev. Lett. **93**, 142502 (2004).
[50] R. Roth and P. Navrátil, Phys. Rev. Lett. **99**, 092501 (2007).
[51] D. A. Varshalovich, A. N. Moskalev, and V. K. Khersonskij, *Quantum Theory of Angular Momentum* (World Scientific, Singapore, 1988).